RESEARCH ARTICLE

BJP | BRITISH PHARMACOLOGICAL SOCIETY

Cognitive improvement via cortical cannabinoid receptors and choline-containing lipids

Marta Moreno-Rodríguez[1] | Jonatan Martínez-Gardeazabal[1] |
Iker Bengoetxea de Tena[1] | Alberto Llorente-Ovejero[1] | Laura Lombardero[1] |
Estibaliz González de San Román[1] | Lydia Giménez-Llort[2] | Iván Manuel[1,3] |
Rafael Rodríguez-Puertas[1,3]

[1]Department of Pharmacology, Faculty of Medicine and Nursing, University of the Basque Country (UPV/EHU), Leioa, Spain

[2]Department of Psychiatry and Forensic Medicine, School of Medicine & Institute of Neuroscience, Autonomous University of Barcelona (UAB), Barcelona, Spain

[3]Neurodegenerative Diseases, BioBizkaia Health Research Institute, Barakaldo, Spain

Correspondence
Marta Moreno-Rodríguez and Rafael Rodríguez-Puertas, Department of Pharmacology, Faculty of Medicine and Nursing. University of the Basque Country (UPV/EHU), Leioa, Spain.
Email: rafael.rodriguez@ehu.es and marta.morenor@ehu.eus

Background and Purpose: Recent research linking choline-containing lipids to degeneration of basal forebrain cholinergic neurons in neuropathological states illustrates the challenge of balancing lipid integrity with optimal acetylcholine levels, essential for memory preservation. The endocannabinoid system influences learning and memory processes regulated by cholinergic neurotransmission. Therefore, we hypothesised that activation of the endocannabinoid system may confer neuroprotection against cholinergic degeneration.

Experimental Approach: We examined the neuroprotective potential of sub-chronic treatments with the cannabinoid agonist WIN55,212-2, using *ex vivo* organotypic tissue cultures including nucleus basalis magnocellularis and cortex and *in vivo* rat models of specific cholinergic damage induced by 192IgG-saporin. Levels of lipids, choline and acetylcholine were measured with histochemical and immunofluorescence assays, along with [^{35}S]GTPγS autoradiography of cannabinoid and muscarinic GPCRs and MALDI-mass spectrometry imaging analysis. Learning and memory were assessed by the Barnes maze and the novel object recognition test in rats and in the 3xTg-AD mouse model.

Key Results: Degeneration, induced by 192IgG-saporin, of baso-cortical cholinergic pathways resulted in memory deficits and decreased cortical levels of lysophosphatidylcholines (LPC). WIN55,212-2 restored cortical cholinergic transmission and LPC levels via activation of cannabinoid receptors. This activation altered cortical lipid homeostasis mainly by reducing sphingomyelins in lesioned animals. These modifications were crucial for memory recovery.

Abbreviations: AA, arachidonic acid; aCSF, artificial cerebrospinal fluid; AD, Alzheimer's disease; BM, Barnes maze; BFCN, basal forebrain cholinergic neurons; DG, dentate gyrus; DHA, docosahexaenoic acid; DIV, days in vitro; DR, discrimination ratio; eCB, endocannabinoid; HMDB, Human Metabolome Database; LPA, lysophosphatidic acid; LPC, lysophosphatidylcholine; LPS, lipopolysaccharide; MALDI-MSI, matrix-assisted laser desorption/ionisation mass spectrometry imaging; MCI, mild cognitive impairment; NBM, Nucleus basalis magnocellularis; NGS, normal goat serum; NORT, novel object recognition test; P7, postnatal day 7; PB, phosphate buffer; PC, phosphatidylcholine; PE, phosphatidylethanolamine; PI, propidium iodide; WT, wild-type.

Conclusion and Implications: We hypothesise that WIN55,212-2 facilitates an alternative choline source by breaking down sphingomyelins, leading to elevated cortical acetylcholine levels and LPCs. These results imply that altering choline-containing lipids via activation of cannabinoid receptors presents a promising therapeutic approach for dementia linked to cholinergic dysfunction.

KEYWORDS

cannabinoids, cholinergic system, lipids, MALDI, memory

1 | INTRODUCTION

The selective vulnerability of basal forebrain cholinergic neurons (BFCN) plays a crucial role in the pathophysiology of dementia in **Alzheimer's disease (AD)** (Grothe et al., 2012, 2013). A significant loss of cholinergic neurons in the nucleus basalis of Meynert and decreased levels of presynaptic cholinergic markers in the neocortex have been described, correlating with cognitive decline in AD (Potter et al., 2011; Whitehouse et al., 1981). Currently, the largest class of drugs approved for the treatment of AD are inhibitors of the enzyme **acetylcholinesterase** (AChE) to increase **acetylcholine** (ACh) at the synaptic cleft, however the clinical benefits of these drugs are limited. Therefore, there is a significant need to develop novel drugs to enhance the functionality of the BFCN projection system especially when damage has already occurred (Moreta et al., 2021). Recently, studies have successfully traced cholinergic pathways in vivo, demonstrating that the integrity of these pathways is disrupted not only in patients with mild cognitive impairment (MCI) and AD but also in individuals with subjective cognitive decline (Nemy et al., 2023; Schumacher et al., 2023).

Given the importance of the above-described cholinergic neurotransmission in AD, animal models of cholinergic dysfunction based on experimental manipulations of the BFCN have been developed as an appropriate tool to study the memory deficits (Rossner, 1997; Schliebs et al., 1996). While the BFCN lesion model does not exhibit the histopathological characteristics of AD such as neurofibrillary tangles and **β-amyloid** plaques, as seen in genetic models of AD like the 3xTg-AD mouse model (Oddo, Caccamo, Kitazawa, et al., 2003), it provides a valuable tool for exploring treatments targeted at improving cognition after cholinergic damage has occurred. Cholinergic neurons have a unique requirement for **choline**, which is utilised in the synthesis of various choline-containing lipids, including phosphatidylcholine (PC), **lysophosphatidylcholine** (LPC), choline plasmalogens and sphingomyelins. These lipids play a crucial role in maintaining the integrity of cholinergic membranes and in the synthesis of the neurotransmitter, ACh (Blusztajn & Wurtman, 1983; Tayebati & Amenta, 2013). The recent description of a close association between choline-containing lipids and BFCN degeneration in AD (Shanks et al., 2022), suggests that, under pathological conditions, the cholinergic system may encounter a dilemma, having to choose between preserving the structural integrity of choline-containing lipids in the membrane and maintaining optimal levels of ACh. Therefore, it is crucial to understand the vulnerabilities

What is already known?

- There is a crosstalk between cannabinoid and cholinergic systems.
- Both systems have a key role in memory.

What does this study add?

- Cannabinoids modify choline-containing lipids.
- Those choline-containing lipids may serve as an additional source of choline.

What is the clinical significance?

- WIN55,212-2 emerges as a potential candidate for addressing memory deficits associated with cholinergic dysfunction.

of the BFCN and explore novel approaches and pathways to maintain the integrity of the cholinergic system.

The endocannabinoid (eCB) system is a neuromodulator system that plays important roles in learning and memory processing, distributed in areas of the brain related to cognition (Harkany et al., 2003) and implicated in cholinergic neurotransmission (Goonawardena et al., 2010; Puighermanal et al., 2012). Cannabinoid agonists induce memory impairment (Broyd et al., 2016; Urits et al., 2021), but in the last decade, evidence has been accumulating showing a beneficial effect of low cannabinoid doses upon cognitive impairment (Bilkei-Gorzo et al., 2017; Calabrese & Rubio-Casillas, 2018; Ozaita & Aso, 2017). The role of the eCB system in neurodegenerative diseases is still unknown. In AD, different studies report changes in the density and activity of **cannabinoid CB$_1$ receptors**, describing an up-regulation or down-regulation in this receptor depending on factors such as disease stage, the animal model or the cohort used and the analysed brain area (Fernandez-Moncada et al., 2023; Lee et al., 2010; Manuel et al., 2014; Moreno-Rodriguez et al., 2024; Mulder et al., 2011). Importantly, the other main subtype of

cannabinoid receptors, the CB$_2$ receptor, is also overexpressed in some AD models and in post-mortem tissue from AD patients, as a key player in β-amyloid-associated microglia (Benito et al., 2003; Medina-Vera et al., 2023; Ruiz de Martin Esteban et al., 2022; Solas et al., 2013). Additionally, a case report revealed that micro-dosing of cannabinoids improved mnemonic learning in a patient with AD (Ruver-Martins et al., 2022). Although some studies showed that cannabinoids modulated the ACh release in the hippocampus and cortex (Gessa et al., 1997; Gessa et al., 1998; Nava et al., 2001), the specific mechanism through which cannabinoids impact or enhance memory remains unknown.

Consequently, to investigate memory deficits and the role of the eCB system in a model of BFCN degeneration, our group previously employed intra-parenchymal injections of the p75^{NTR}-binding 192IgG-Saporin toxin into the nucleus basalis magnocellularis (NBM) in rats. The studies showed that after the lesion, rats showed memory impairment, increased levels of CB$_1$ receptor activity (Llorente-Ovejero et al., 2017) and altered levels of choline-containing lipids (Llorente-Ovejero et al., 2021) in both the NBM and cortex. These results suggested that choline-containing lipids and the eCB system play a key role in the specific degeneration of basal forebrain-cortical cholinergic circuits. These findings led us to use cannabinoid agonists as a therapeutic approach to treat cholinergic deficits. In this study, we have used the in vivo animal model of BFCN degeneration to present evidence of an alternative cellular source of choline that uses the synthetic cannabinoid WIN55,212-2 to restore ACh levels, the choline-containing lipids, to induce cognitive improvement.

2 | METHODS

2.1 | Animals

All animal care and experimental procedures were in accordance with European animal research laws (Directive 2010/63/EU) and the Spanish National Guidelines for Animal Laws (RD 53/2013, Law 32/2007) and were approved by the Local Ethics Committee for Animal Research of the University of the Basque Country (CEEA M20-2018-52 and 54). Animal studies are reported in compliance with the ARRIVE guidelines (Percie du Sert et al., 2020) and with the recommendations made by the *British Journal of Pharmacology* (Lilley et al., 2020).

Ex vivo hemibrain organotypic cultures were derived from 25 male Sprague–Dawley rats' postnatal day 7 (P7), weighing 14–20 g, and for the in vivo experimental model, 121 adult male Sprague–Dawley rats, weighing 200–250 g, were used for 192IgG-saporin or vehicle administration. All rats were housed in cages (50-cm length × 25-cm width × 15-cm height), four or five per cage, at 22°C in a humidity-controlled (65%) room with a 12:12-h light/dark cycle, with access to food and water ad libitum. Seven-month-old C57BL/6 male 3xTg-AD mice (n = 17) harbouring PS1$_{M146V}$, APP$_{Swe}$ and Tau$_{P301}$L genes provided by Prof. Lydia Giménez-Llort from Universitat Autònoma de Barcelona and age-matched wild-type C57BL/6 (n = 20) from Envigo (Indianapolis, IN, USA) weighing 25–30 g were also used. Mice were housed in groups of 3–4 per cage at a temperature of 22°C and in a

humidity-controlled (65%) room with a 12:12-h light/dark cycle, with access to food and water ad libitum.

Every effort was made to minimise the discomfort of the animals and to use the minimum number of animals. The study is focused exclusively on male rodents to avoid the significant effects of fluctuations in hormonal levels, particularly oestrogen and progesterone, which are derived from lipids; therefore, further experiments in female animals should report interesting findings.

2.2 | Ex vivo model of cholinergic degeneration in organotypic cultures and cannabinoid treatments

P7 Sprague–Dawley rats were killed by decapitation and brains were quickly dissected under aseptic conditions inside a laminar flow cabinet. The protocol used was described in detail by Llorente-Ovejero et al. (2021). In brief, approximately six slices containing cholinergic neurons within the NBM were obtained from each brain, and these were immediately transferred into cell culture inserts over membranes of 0.4-μm pore size (PIC50ORG, Millipore, MA, USA), placed in six-well culture dishes (Falcon, BD Biosciences Discovery Labware, Bedford, MA) containing cell culture medium. The culture medium consisted in 49% (v/v) neurobasal medium (NB, Sigma-Aldrich), 24% (v/v) Hanks' balanced salt solution (HBSS, Gibco), 24% (v/v) normal horse serum (NHS, Gibco), 1% (v/v) d-glucose, 0.5% glutamine (Sigma-Aldrich), 0.5% B27 supplement serum free (Gibco) and 1% antibiotic/antimycotic. The culture plates were incubated at 37°C in a fully humidified atmosphere supplemented with 5% CO$_2$. The ex vivo hemibrain organotypic cultures were randomly divided into two groups: in group 1 fresh cell culture medium was added. In group 2 fresh cell culture medium containing 192IgG-saporin (100 ng/ml) was added on Days 2 and 5 in vitro (DIV). Both groups were treated with WIN55,212-2 (1 nM or 10 nM) dissolved in ethanol. The maximum final ethanol concentration in culture medium was set at 0.01% (v/v), according to previous reports (Koch et al., 2011). To verify receptor specificity of the effect exerted by the cannabinoid agonist WIN55,212-2, a third group of animals were treated as those in group 2 with the addition of the CB$_1$ receptor antagonist AM251 (1 μM) (Koch et al., 2011). After 8 DIV, organotypic cultures were incubated in the presence of 5 μg·ml^{-1} of propidium iodide (PI) to mark degenerating cells (bright red) for 2 h prior to fixation with paraformaldehyde. The ex vivo outcomes were assessed under blinded conditions; the data analyst was unaware of the treatment assignments for each group.

2.3 | In vivo rat model of basal forebrain cholinergic degeneration and cannabinoid treatments

Basal forebrain cholinergic degeneration was induced following bilateral stereotaxic (−1.5 mm anteroposterior from Bregma, ±3 mm mediolateral from midline, +8 mm dorsoventral from cranial surface) injection of 192IgG-saporin (130 ng·μl^{-1}) into the NBM, as previously described (Llorente-Ovejero et al., 2017). Control rats received an injection of artificial cerebrospinal fluid (aCSF) into the NBM. Rats

were allowed to recover from surgery for 7 days. On Day 8, we initiated treatments and training on the Barnes maze (BM) and novel object recognition test (NORT), as described below.

In the BM performance, aCSF and 192IgG-SAP groups received i.p. injections of WIN55,212-2 (0.5 or 3 mg·kg^{-1}) or vehicle solution (1:1:18; DMSO:Kolliphor: saline) for five consecutive days, 1 h prior to the performance of the task. To verify receptor specificity of the cannabinoid effect, another group of animals received an i.p. injection of WIN55,212-2 (0.5 mg·kg^{-1}) along with CB_1 receptor antagonist SR141716A (0.5 mg·kg^{-1}, i.p.). WIN55,212-2 and SR141716A were administered sequentially, one after the other, both 1 h before behavioural performance. Rats were randomly selected for each group: (n = 28) aCSF; (n = 12) aCSF + W0.5; (n = 8) aCSF + W3; (n = 7) aCSF + SR; (n = 30) 192IgG-SAP; (n = 12) 192IgG-SAP + W0.5; (n = 8) 192IgG-SAP + W3; (n = 9) 192IgG-SAP + W + SR; (n = 9) 192IgG-SAP + SR.

In the NORT performance, WIN55,212-2 (0.5 mg·kg^{-1}, i.p., 5 days) was administered daily for five consecutive days, 1 h before each phase of the behavioural test. Different groups of rats were used for the BM test because using the same animals for different tests can alter the outcomes, as previously reported by our group (Bengoetxea de Tena et al., 2022), making it unsuitable for consistent memory measurement. The following groups of rats were used: control group aCSF (n = 10), aCS + WIN0.5 (n = 10), 192IgG-saporin (n = 10) and 192IgG-SAP + W0.5 group (n = 10). Animals were killed by decapitation 3 days after the last WIN55,212-2/vehicle administration. The decision to wait for 3 days between behavioural testing and tissue measures was based on the requirements of autoradiography studies. These studies demand a washout period to ensure that the brain is free from drug interference deriving from the compounds administered in vivo, thus ensuring accurate experimental outcomes.

The in vivo outcomes were assessed under blinded conditions; the data analyst was unaware of the treatment assignments for each group.

2.4 | WIN55,212-2 administration in the 3xTg-AD mouse model of familial AD

Given that the loss of basal forebrain cholinergic projections is an early feature of AD, we studied if the same cannabinoid treatment would also be beneficial in an animal model of familial AD, the 3xTg-AD mouse, which shows the histopathological hallmarks of the disease (Oddo, Caccamo, Shepherd, et al., 2003). WIN55,212-2 (0.1 mg·kg^{-1}, equivalent to 0.5 mg·kg^{-1} in rats, i.p., 5 days) (Nair & Jacob, 2016) was administered daily for five consecutive days, 1 h before each phase of BM test to 3xTg-AD and age-matched wild-type C57BL/6 mice. The following groups of animals were used: control group (WT, n = 10), WIN55,212-2 (0.1 mg·kg^{-1}) group (WT + WIN0.1, n = 10), 3xTg-AD group (3xTg-AD, n = 8) and 3xTg-AD + WIN55,212-2 (0.1 mg·kg^{-1}) group (3xTg-AD + WIN0.1, n = 9), only tested in BM and not in NORT.

2.5 | Barnes maze

This test was performed using two white circular platforms, one for rats (130 cm of diameter, 100 cm from the floor, 20 holes 10 cm each and 2.5 cm between holes) and one for mice (92 cm of diameter, 100 cm from the floor, 20 holes 5 cm each and 2.5 cm between holes). Only one of the holes leads to a dark chamber located under it. Two bright lights (400 W, approximately 1310 luxes light condition) and visual cues were placed around the platform. Each rodent was placed in the middle of the maze and was allowed to explore the maze for 3 min. If a rodent did not reach the target hole in the given 3 min, it was gently guided to it. During 4 days of training, rodents conducted four trials per day, with 15 min between trials. During the training days, total latency (the time to reach the target hole) was measured. A gradual decrease in this parameter over the four training days is indicative of spatial memory. On Day 5, the target hole was closed, and rodents were allowed to explore the maze for 3 min. As an additional measure of spatial memory, time in the target quadrant (the quadrant where the target hole was located) was measured. The maze was cleaned using a 10% ethanol solution after every trial. All the procedures were analysed by SMART 3.0 video tracking software (Panlab Harvard apparatus, Barcelona, Spain, RRID:SCR_002852).

2.6 | Novel object recognition test

The novel object recognition test (NORT) was performed in a white open-field arena (90 × 90 × 50 cm) (Panlab S.L., Barcelona, Spain) in a room under one lux light condition. A video camera placed above the shuttle box recorded the behaviour of the rats. The test was divided into four distinct phases that were carried out throughout 5 days: habituation phase (3 days), familiarisation phase, short-term testing (5 h after familiarisation) and long-term testing (24 h after familiarisation). Before each phase, rats were transported to the experimental room for about 10 min and each rat was gently handled individually for 1 min, having its neck and back stroked by the experimenter's fingers, before entering the arena. After leaving the arena, rats were gently handled again. Habituation phase lasted for 3 days and consisted in placing rats in the arena to allow them to explore the compartment for 5 min. In the familiarisation phase, which was carried out on the fourth day, rats were presented with two identical objects (Object A and Object A), built with five to six mega blocks, with a height of about 10 cm. The objects were positioned diagonally in opposite corners of the arena, approximately 10 cm away from their respective walls, and were mirror images of each other. To avoid possible bias regarding the location of the objects, these were rotated after the familiarisation phase of each rat. A 25-s exploration threshold for both objects combined was established and rats remained in the arena until that threshold was met. If rats failed to reach the 25-s exploration threshold in 15 min, they were excluded from the study. Exploration of the objects was considered when the rats touched the object or faced it with their nose being less than 2 cm away from it. Five hours after the familiarisation phase, short-term testing was

performed. In that phase, rats were again placed in the arena and were presented with one of the familiar objects (Object A) and with a new object (Object B). Rats were given 5 min to explore the objects. Twenty-four hours after the familiarisation phase, on the fifth day, long-term testing was performed. Rats were again placed in the arena and were presented with the familiar object (Object A) and a third, new object (Object C). Rats were given 5 min to explore the objects. In the first habituation phase, which is equivalent to an open field test, the total path length of the rats and their speed were measured using an automated tracking system (SMART, Panlab S.L., Barcelona, Spain) as indicators of exploratory behaviour. In the short and long-term testing phases, the amount of time dedicated to exploring the familiar and new objects was measured and the object discrimination ratio (DR) was calculated using the following formula: DR = [(novel object exploration time − familiar object exploration time)/total exploration time]. A higher DR was indicative of more time exploring the new object compared to the familiar one and was thus considered a positive performance in the test (good recognition memory). DR scores approaching zero reflect no preference for the new object and negative scores indicate preference for the familiar object, which reflect impairment of recognition memory in both cases. Moreover, the total exploration time spent by the rats in short- and long-term testing phases was measured to investigate the effect of the different model, or the drugs administered on object exploration.

2.7 | Tissue preparation

Organotypic cultures on Day 8 were gently and extensively rinsed with 0.9% saline solution (37°C) followed by immersion in 4% paraformaldehyde and 3% picric acid in 0.1 M PB (4°C) for 1 h. Groups of animals which had been tested on the BM, on Day 15 after the lesion, were anaesthetised with ketamine/xylazine (90/10 mg·kg^{-1}; i.p.) and killed by decapitation or transcranial perfusion to obtain fresh or fixed tissue, respectively. Fresh brains from experimental groups (n = 96) were quickly removed by dissection, fresh frozen, and kept at −80°C. Later, brains were cut into 20 μm coronal sections using a Microm HM550 cryostat (Thermo Scientific, Waltham, MA, USA) equipped with a freezing-sliding microtome at −25°C and mounted onto gelatin-coated slides and stored at −25°C. Animals from experimental groups (n = 25) were transcardially perfused with 50 ml of warm (37°C), calcium-free Tyrode's solution (0.15 M NaCl, 5 mM KCl, 1.5 mM MgCl$_2$, 1 mM MgSO$_4$, 1.5 mM NaH$_2$PO$_4$, 5.5 mM glucose, 25 mM NaHCO$_3$; pH 7.4), 0.5% heparinized, followed by 4% paraformaldehyde and 3% picric acid in 0.1 M phosphate buffer (PB) (4°C) (100 ml per 100 g; 37°C, pH 7.4). Brains were removed and placed in a cryoprotective solution consisting of 20% sucrose in PB overnight at 4°C, and frozen by immersion in isopentane and kept at −80°C. Brains were cut into 12-μm coronal sections as described above, mounted onto gelatin-coated slides and stored at −25°C until used for the immunofluorescence assays.

Fresh frozen sections were used for [^{35}S]GTPγS autoradiography, AChE detection and MALDI-mass spectrometry imaging analysis. The remaining brain sections were dissected to isolate the cortical area for choline/acetylcholine assays, rat brain cortex incubation and MALDI-MS analysis. Fixed sections were only used for immunofluorescence assays.

2.8 | Immunofluorescence

The immunofluorescence studies complies with the BJP guidelines for immunoblotting and immunohistochemistry (Alexander et al., 2018). Organotypic culture sections were blocked and permeabilised with 4% normal goat serum (NGS) with 0.6% Triton X-100 in PBS (0.1 M, pH 7.4) for 2 h at 4°C. The incubation was performed using the free-floating method at 4°C (48 h) with rabbit anti-p75^{NTR} (1:500; Cell signalling, MA, USA, Cat# 4201, RRID:AB_1904041) with 0.6% Triton X-100 in PBS with 5% BSA. The primary antibody was then revealed by incubation for 30 min at 37°C in darkness with donkey anti-rabbit Alexa 488 (1:250; Thermo Scientific, Waltham, MA, USA, Cat# A-21206, RRID:AB_2535792) with Triton X-100 (0.6%) in PBS. For the processing of fixed rat tissue, 12-μm coronal sections were blocked and permeabilised with 3% donkey serum with 0.25% Triton X-100 PBS (0.1 M, pH 7.4) and 2 h later they were labelled with mouse anti-Iba1 (1:500; Fujifilm Wako Chemicals, VA, USA, Cat# 016–26,721, RRID:AB_2811160) or rabbit anti-p75^{NTR} (1:750; Cell signalling, MA, USA, Cat# 4201, RRID:AB_1904041) overnight. After several washes, the appropriate secondary antibody (1:200) was applied (Donkey anti-rabbit Alexa fluor-488 Cat# A-21206, RRID:AB_2535792 for p75^{NTR} and donkey anti-mouse Alexa fluor-555 Cat# A-31570, RRID:AB_2536180 for Iba1; Thermo Scientific, Waltham, MA, USA) for 2 h. Controls of immunofluorescence consisted in primary antibody omission resulting in the absence of immunoreactivity.

2.9 | Cells quantitation

In organotypic cultures, 200-fold magnification photomicrographs of the BFCNs within the NBM were acquired by means of an Axioskop 2 Plus microscope (Zeiss) equipped with a CCD imaging camera (SPOT Flex Shifting Pixel). Both p75^{NTR} immunoreactive and PI positive cells were stereologically counted and the total number of cells in the whole image was reported. The population of p75^{NTR} immunoreactive or PI-stained cells was expressed as p75^{NTR} or PI cells·mm^{-2}. In rat tissue, 200-fold magnification photomicrographs of NBM in both hemispheres were randomly acquired by Axioskop 2 Plus microscope (Carl Zeiss) equipped with a CCD imaging camera SPOT Flex Shifting Pixel. p75^{NTR} immunoreactive positive cells were stereologically counted at three different stereotaxic levels (−1.20, −1.56 and −1.92 mm from Bregma), in six different rats per group and the total number of cells in the whole image was obtained. The density of cholinergic cells was expressed as p75^{NTR} positive cells·mm^{-3}. Iba1 immunoreactive positive cells were counted at stereotaxic level −1.56 mm from Bregma, in three different rats per

group and the total number of cells in the whole image was obtained. The number of Iba1 positive cells was expressed as cells·mm^{-2}.

2.10 | MALDI-MSI

Matrix-assisted laser desorption/ionisation mass spectrometry imaging (MALDI-MSI) was performed using fresh 20-µm sections for each sample. MBT matrix was deposited on the tissue surface by sublimation. The sublimation was performed using 300 mg of MBT, and the deposition time and temperature were controlled (23 min, 100°C). For the recrystallisation of the matrix, the sample was attached to the bottom of a glass Petri dish face-down, which was placed on another Petri dish containing a methanol-impregnated piece of filter paper on its base. The Petri dish was then placed on a hot plate (1 min, 38°C) (Martinez-Gardeazabal et al., 2023). A MALDI LTQ-XL-Orbitrap (Thermo Fisher Scientific, San Jose, CA, USA) equipped with a nitrogen laser (λ = 337 nm, rep rate = 60 Hz, spot size = 80 µm × 120 µm) was used for mass analysis. Thermo's Image-Quest software was used to analyse MALDI-MSI data and image acquisition in positive ion mode. The used range was 400–1000 Da with 10 laser shots per pixel at a laser fluence of 15 µJ. The target plate stepping distance was set at 150 µm for both *x*- and *y*-axes by the MSI image acquisition software. The data were normalised using the total ion current values. Each of the *m/z* values was plotted for signal intensity for each pixel (mass spectrum) across a given area (tissue section) using MSiReader software (Robichaud et al., 2013). The *m/z* range of interest was normalised using the ratio of the total ion current for each mass spectrum. The data were expressed as absolute intensity in arbitrary units. The assignment of lipid species was facilitated using the databases Lipid MAPS (http://www.lipidmaps.org/) and the Human Metabolome Database (HMDB) (https://hmdb.ca). The 5-ppm mass accuracy was selected as the tolerance window for the assignment.

2.11 | [^{35}S]GTPγS autoradiography

Fresh 20-µm slices from all experimental groups were dried, followed by two consecutive incubations in HEPES-based buffer (Sigma-Aldrich, St. Louis, MO, USA) (50-mM HEPES, 100-mM NaCl, 3-mM MgCl$_2$, 0.2-mM EGTA and 0.5% BSA, pH 7.4) for 30 min at 30°C to remove endogenous ligands. Then, slices were incubated for 2 h at 30°C in the same buffer but supplemented with 2-mM GDP, 1-mM DTT, adenosine deaminase (3 units·L^{-1}) and 0.04 nM [^{35}S]GTPγS. Basal binding was determined in two consecutive slices in the absence of the agonist. The agonist-stimulated binding was determined in another consecutive slice with the same reaction buffer, but in the presence of the corresponding receptor agonists, CP55,940 (10 µM) for CB$_1$ receptors and carbachol (100 µM) for muscarinic M$_2$/M$_4$ receptors (mAChR M$_2$/M$_4$). Non-specific binding was defined by competition with non-radioactive GTPγS (10 µM) in another

section. Then, slices were washed twice in cold (4°C) 50-mM HEPES buffer (pH 7.4), dried and exposed for 48 h to *β*-radiation sensitive film with a set of [^{14}C] standards (American Radiolabeled Chemicals, St. Louis, MO, USA) calibrated for [^{35}S].

2.12 | Histochemistry for AChE detection

Fresh 20-µm slices from all experimental groups were air dried and post-fixed with 4% paraformaldehyde for 30 min at 4°C. Slices were rinsed twice in 0.1 M Tris-maleate buffer (pH 6.0) for 10 min and incubated in the AChE reaction buffer: 0.1 M Tris-maleate; 5-mM sodium citrate; 3-mM CuSO$_4$; 0.1-mM iso-OMPA; 0.5 mM K$_3$Fe(CN)$_6$ and 2-mM acetylthiocholine iodide as reaction substrate. The incubation time to stain cholinergic fibres was 100 min. The enzymatic reaction was stopped by two consecutive washes (2 × 10 min) in 0.1 M Tris-maleate (pH 6.0). Slices were then dehydrated in increasing concentrations of ethanol and covered with DPX as the mounting medium. Finally, the stained slices were scanned at 600 ppi resolution, the images were converted to 8-bit grey-scale mode and AChE positive fibre density was quantified by Image J software (NIH, Bethesda, MD, USA). Software measured the optical density (O.D.) of AChE reactivity in each anatomical area.

2.13 | Rat brain cortex incubation

Samples (10mg) of fresh cortical tissue (motor cortex M1/2 and somatosensorial cortex S1) were collected, washed in cold PBS and resuspended in 500 µl of choline/acetylcholine assay kit choline assay buffer (Abcam, Cambridge, UK, Cat# ab65345). The tissue was homogenised with a homogeniser (Heidolph RZR 50 Homogeniser 300–2000 RPM w/Barnant 50001-92 Stand 115V), sitting on ice, with 10–15 passes. The samples were incubated in choline assay buffer at 37°C and collected every 15 min, for 2 h. After incubation, samples were centrifuged at 25,258 x *g* for 5 min at 4°C. Supernatants were collected to use them with the choline/acetylcholine assay buffer and dry pellets were analysed by MALDI-MS.

2.14 | Choline/acetylcholine assay

Choline and acetylcholine were quantified in rat cortical tissue (motor cortex M1/2 and somatosensorial cortex S1) from all experimental groups using a choline/acetylcholine assay kit (Abcam, Cambridge, UK, Cat# ab65345). Fresh cortical tissue (10 mg) were harvested, washed in cold PBS and resuspended in 500 µl of choline assay buffer. The tissue was homogenised with a homogeniser (Heidolph RZR 50 Homogenizer 300–2000 RPM w/Barnant 50001-92 Stand 115V), sitting on ice, with 10–15 passes. Samples were centrifuged at 25,258 x *g* for 5 min at 4°C. Supernatants were collected and used with the choline/acetylcholine assay buffer. The assay was carried out in accordance with the manufacturer's instructions, in the absence

and presence of acetylcholinesterase to identify values of total and free choline, which allowed an indirect quantification of acetylcholine. The relative sample fluorescence was determined using Varioskan LUX Reader (Thermo Scientific, Waltham, MA, USA).

2.15 | Cortical sample preparation for MALDI-MS

Cortical lipid composition was analysed in all experimental groups by MALDI-MS. Dry pellets from rat cortical tissue (motor cortex M1/2 and somatosensorial cortex S1) from all experimental groups were obtained and the protein concentration was determined using the Bradford method. Samples were reconstituted with water at the same concentration. A mixed sample (3 μl of sample and 7 μl of matrix-saturated solution of MBT) was deposited on a MALDI plate containing 96 wells, using the dried droplet method. Xcalibur software was used for MALDI data acquisition in both positive and negative ion modes. The positive ion range was 400–1,000 Da, and the negative ion range was 400–1100 Da, with 3 min of shots per well at a laser fluence of 15 μJ. The m/z range of interest was normalised using the ratio of the total ion current for each mass spectrum. The data were expressed as absolute intensity in arbitrary units. The assignment of lipid species was facilitated using the databases Lipid MAPS (http://www.lipidmaps.org/, RRID:SCR_003817) and the Human Metabolome Database (HMDB, https://hmdb.ca, RRID:SCR_007712). The 5-ppm mass accuracy was selected as the tolerance window for the assignment.

2.16 | Data and statistical analysis

The data and statistical analysis comply with the recommendations of the *British Journal of Pharmacology* on experimental design and analysis in pharmacology (Curtis et al., 2022). For the in vitro, statistical analysis was performed only when the group size was n ≥ 5 independent values. In vivo studies the variability in sample numbers in behavioural studies arises from the diverse preparation methods of tissue, whether frozen or fixed. The groups were designed to generate of equal size and the variation in group size within an experiment was due to unexpected death of animals. Statistical analysis was performed only for studies where each group size was at least n ≥ 5 independent values. Data are expressed as mean ± SEM. Although some of our data met the assumptions for parametric analysis, the small sample size (<20) made non-parametric statistics more appropriate for accurate results. Data evaluated across the groups used the Kruskal–Wallis test followed by Dunn's post hoc tests for multiple comparisons. Spearman rank for correlations (SigmaPlot 12.5, RRID:SCR_003210) and false discovery rate were used to adjust for multiple comparisons between correlations. Statistical significance was set at $P < 0.05$ (two tailed). However, a two-way repeated measures ANOVA was used only for the learning data in the BM, followed by Tukey's multiple

comparisons post hoc test. Statistics and data were graphically represented using GraphPad Prism 9 (GraphPad Software, RRID: SCR_002798). The heat map generation was performed using the freely available software programme Heatmapper (http://www.heatmapper.ca/). Additionally, blinding procedures were implemented throughout all the experiments to minimise bias and enhance the validity of the results.

2.17 | Materials

192IgG-saporin (Cat# MAB390, RRID:AB_94979) was from Millipore (Temecula, CA, USA); AM251 and SR141716A were supplied by Tocris Bioscience (Bristol, UK). Acetylthiocholine iodide, adenosine deaminase, carbachol, CP55,940, GTPγS and WIN55,212-2 were supplied by Sigma-Aldrich (St. Louis, MO, USA); [^{35}S] GTPγS (1250 Ci·mmol^{-1}) was supplied by PerkinElmer (Boston, MA, USA).

2.18 | Nomenclature of targets and ligands

Key protein targets and ligands in this article are hyperlinked to corresponding entries in http://www.guidetopharmacology.org, and are permanently archived in the Concise Guide to PHARMACOLOGY 2021/22 (Alexander, Christopoulos, et al., 2023; Alexander, Fabbro, et al., 2023).

3 | RESULTS

3.1 | WIN55,212-2 protects cell viability after BFCN degeneration in organotypic cultures

PI uptake was quantified as a measure of cell death in the NBM after treatment with 192IgG-saporin and different cannabinoid treatments in rat postnatal day 7 (P7) hemibrain organotypic cultures. Ex vivo application of 100 ng·ml^{-1} of the toxin 192IgG-saporin at days two and five produced a significant increase in the density of PI-stained cells (PI+ cells·mm^{-2}; control, 14.22 ± 2; 192IgG-saporin: 63.3 ± 7. Figure S1a,c). Pretreatment of organotypic cultures with either 1 or 10 nM of WIN55,212-2, 2 h prior to the application of 192IgG-saporin, induced protective effects on cell viability (192IgG-saporin: 63.3 ± 7; 192IgG-saporin + W [10 nM]: 17.78 ± 7. Figure S1a,c). p75^{NTR+} cells in the same area were counted as a specific marker of cholinergic neurons. The application of the immunotoxin at days two and five led to a statistically significant decrease in the density of cholinergic cells in NBM (p75^{NTR+} cells·mm^{-2}; aCSF: 61.87 ± 4 ; 192IgG-SAP: 26.22 ± 7. Figure S1b,c), while pretreatment of cultures with either dose of WIN55,212-2, 2 h prior to the application of the toxin, did not change the number of p75^{NTR+} cells.

3.2 | WIN55,212-2 restored spatial and recognition memory on an in vivo model of cholinergic degeneration

In the Barnes Maze (BM), a progressive reduction in the total latency of the experimental groups indicates proper memory function during the acquisition training (Figure 1a). On the probe day, lesioned animals spent significantly less time in the target quadrant compared to the control group (Figure 1b,c), showing memory impairment after toxin administration. Administration of either dose of WIN55,212-2 (0.5 and 3 mg·kg^{-1}) after the BFCN lesion increased the time in the target quadrant, reaching control levels (Figure 1c). Co-treatment with SR141617A, a specific CB$_1$ receptor antagonist, blocked the cognitive improvement following WIN55,212-2, indicating that cognitive restoration was mediated by the
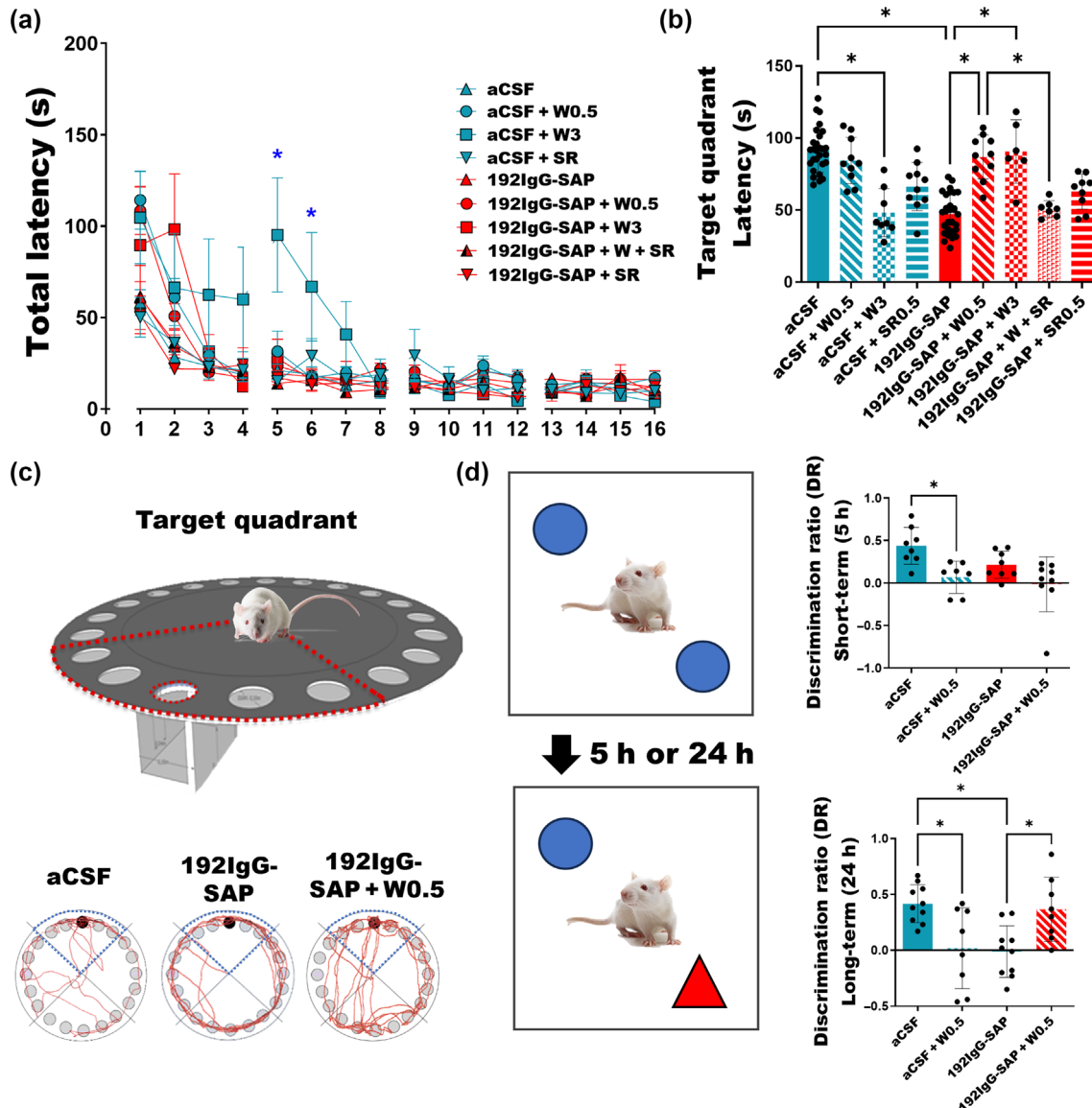

FIGURE 1 WIN55,212-2 improved cognitive impairment evaluated by BM and NORT following BFCN lesion. (a) Analysis of the total latency, which is the time spent by the rats to reach the target hole during 16 trials throughout 4 days for all the groups. Data shown are means ± SEM. *$P < 0.05$, significantly different as indicated; two-way repeated measures ANOVA followed by a Tukey's multiple comparisons post hoc test. (b) Time in target quadrant of the rats on day 5, which is the time spent in the target quadrant. aCSF, aCSF + W0.5, 192IgG-SAP + W0.5 and 192IgG-SAP + W3 spent more time in target quadrant than the rest of experimental groups. Data shown are individual values with means ± SEM. *$P < 0.05$, significantly different as indicated; Kruskal–Wallis test, post hoc test Dunn's multiple comparison; (n = 28) aCSF; (n = 12) aCSF +W0.5; (n = 8) aCSF + W3; (n = 7) aCSF + SR; (n = 30) 192IgG-SAP; (n = 12) 192IgG-SAP + W0.5; (n = 8) 192IgG-SAP + W3; (n = 9) 192IgG-SAP + W + SR; (n = 9) 192IgG-SAP + SR. (c) Image of the Barnes Maze with the target quadrant delineated in red and the trajectories of aCSF, 192IgG-SAP and 192IgG-SAP + W0.5 groups. (d) On the left a scheme depicting a simplified version of the protocol followed for the assessment by NORT. On the right total exploration time of the objects in the short-term and the long-term for aCSF, aCSF + W0.5, 192IgG-SAP and 192IgG-SAP + W0.5. Data shown are individual values with means ± SEM. *$P < 0.05$, significantly different as indicated; Kruskal–Wallis test with post hoc test Dunn's multiple comparison; (n = 10) aCSF; (n = 9) aCSF + W0.5; (n = 10) 192IgG-SAP; (n = 8) 192IgG-SAP + W0.5.
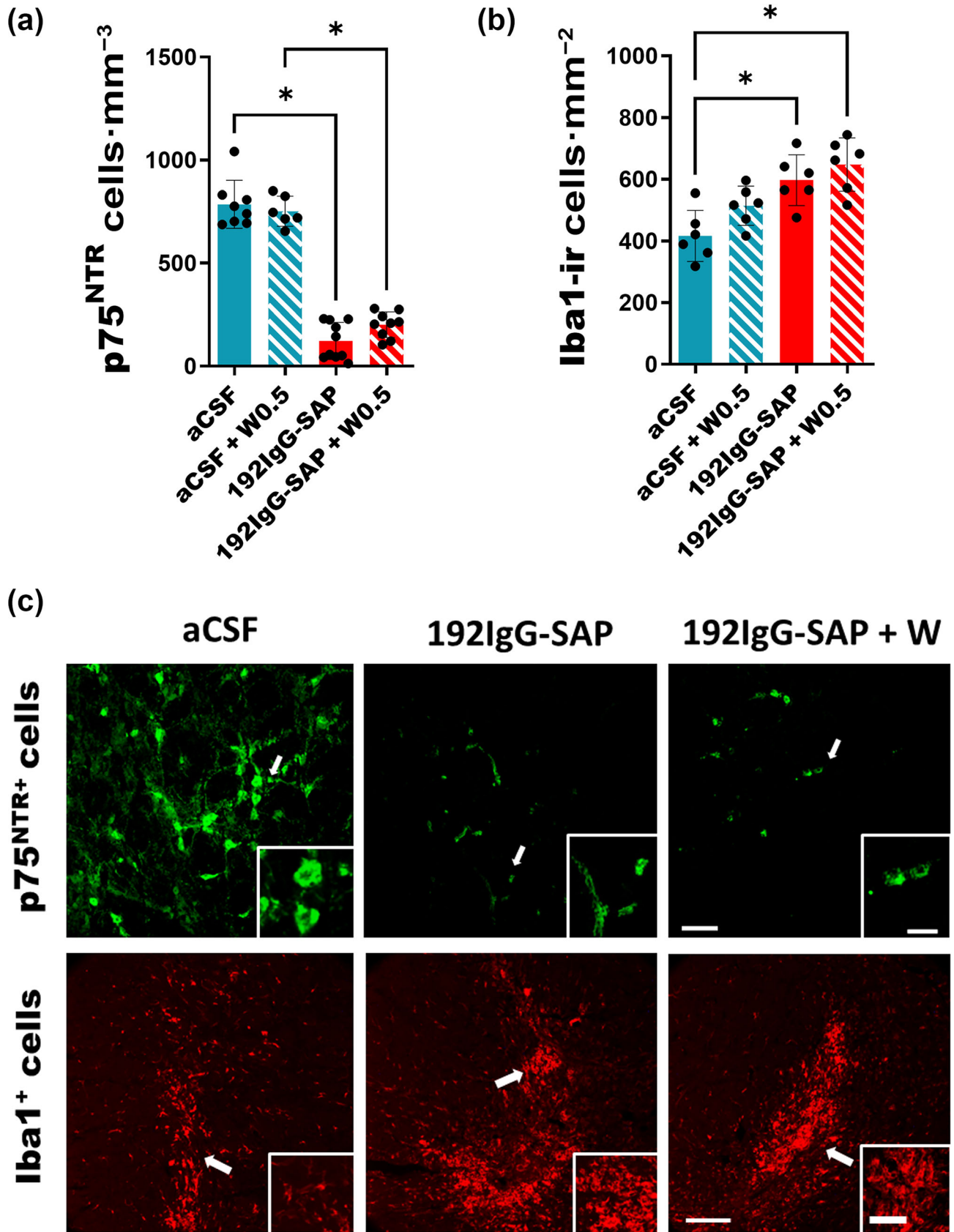
FIGURE 2 Legend on next page.

FIGURE 2 Immunofluorescent studies of (a) p75^{NTR} and (b) Iba1 positive cells of aCSF, 192IgG-SAP, aCSF + W and 192IgG-SAP + W groups in the NBM. (c) Labelling images of p75^{NTR} positive cells (green) and Iba1 positive cells (red) of aCSF, 192IgG-SAP and 192IgG-SAP+W (0.5 mg·kg^{-1}) group. Note that 192IgG-SAP group had less p75^{NTR} positive cells (cholinergic cells) but had more Iba1 positive cells (microglia). WIN55,212-2 treatment did not modify cell number. Scale bar 100 μm (inset 50 μm) for p75^{NTR} and scale bar 100 μm (inset 25 μm) and Iba1 images. Data shown are individual values with means ± SEM; Iba1: n = 6; p75^{NTR}: n = 8. *$P < 0.05$, significantly different as indicated; Kruskal–Wallis test with post hoc test Dunn's multiple comparison.

activation of CB$_1$ receptors. Interestingly, the high dose of WIN55,212-2 produced opposite effects: cognitive function was improved in lesioned rats, while it was impaired in control rats (Figure 1c). We conducted additional experiments using a single acute dose of WIN55,212-2 on day 5 of Barnes maze. Lesioned animals exhibited cognitive impairment with only one dose of WIN55,212-2 (0.5 mg·kg^{-1}), whereas the control group did not show any memory deficit in the probe trial (unpublished data). To complete this study, we employed the most effective dose from the BM, 0.5 mg·kg^{-1}, to analyse the discrimination ratio in the novel object recognition test (NORT) in both the short-term (5 h post-familiarisation with the objects) and the long-term (24 h post-familiarisation). In the short-term, sub-chronic treatment with WIN55,212-2 impaired memory in control rats (Figure 1d), as already observed with the high dose of 3 mg·kg^{-1} in the BM. Short-term recognition memory was relatively preserved in the 192IgG-SAP group. In the long-term test, WIN55,212-2 clearly impaired recognition memory in control rats as measured by a decrease in the discrimination ratio (DR), while 192IgG-SAP caused a significant decrease in the DR in the long-term (Figure 1d), indicating recognition memory impairment following the depletion of BFCNs in the long-term, but not in the short-term. Importantly, administration of WIN55,212-2 to lesioned rats improved memory in the NORT test in the long-term, increasing the DR to control levels (Figure 1d).

In the 3xTg-AD mouse model, WIN55,212-2 was administered to both wild-type (WT) and 3xTg-AD mice at a dose of 0.1 mg·kg^{-1}, equivalent to 0.5 mg·kg^{-1} in rats (Nair & Jacob, 2016). The time to reach the target hole during each trial showed significant differences between the groups. On Day 4 of the acquisition phase, both WT and 3xTg-AD mice showed reduced total latencies, indicating a correct learning process for both phenotypes, which was significantly slower for 3xTg-AD mice, suggesting mild spatial cognitive deficits at 7 months of age in this AD model. WIN55,212-2 administration in WT mice induced a deleterious effect on learning, while in 3xTg-AD mice, the treatment did not reverse the observed cognitive deficits (Figure S2a). In the probe trial, no statistically significant differences were observed between groups (Figure S2b).

3.3 | WIN55,212-2 did not modify the glial response following the administration of 192IgG-saporin

Glial activation following a lesion of the NBM was analysed in the aCSF, 192IgG-SAP, aCSF + W0.5 and 192IgG-SAP + W0.5 groups. Following 192IgG-saporin administration, quantification revealed a significant decrease in the number of p75NTR+ cells (Figure 2a,c), while the number of Iba1-positive cells increased (Figure 2b,c). After

WIN55,212-2 administration, the number of p75^{NTR} or Iba1-positive cells at the lesion site was not modified (Figure 2a–c). Given the anti-inflammatory properties of cannabinoids and to describe potential changes in microglial phenotype or activation states (Blank et al., 2022), microglial inflammation-associated lipid biomarkers in the same experimental groups were evaluated by MALDI-MSI (Table S1). Following the lesion, a significant increase in lysophosphatidylcholines (LPC) C18 and C16 (LPC 18:0 a.u.; Control: 55207 ± 13,922 vs. 192IgG-SAP: 144700 ± 19,651, LPC 16:0 a.u.; Control: 13808 ± 3,085 vs. 192IgG-SAP: 51672 ± 14,782), sphingomyelin (SM 34:1 a.u.; Control: 14531 ± 4,591 vs. 192IgG-SAP: 38556 ± 4,956) and palmitoyl (CAR 16:0) and oleoyl carnitine (CAR 18:1) levels were described at the lesion site (CAR 16:0; Control: 9893 ± 4,149 vs. 192IgG-SAP: 65156 ± 8,637; CAR18:1; Control: 8120 ± 5,517 vs. 192IgG-SAP: 421720 ± 93,521), while C32-phosphatidylcholines (PC 32:0) did not show a significant reduction. This lipidomic analysis indicated that lipids associated with the microglial inflammatory response were increased at the lesion site. For example, sphingomyelin 34:1, which is restricted to the choroid plexus in the control group, was detected at the lesion site following immunotoxin administration. Acyl-carnitines, which were only slightly detected in control rats, were significantly increased at the lesion site following administration of the immunotoxin (Figure S3).

3.4 | WIN55,212-2 increased cortical muscarinic and cannabinoid receptor activity

The activity elicited by CB$_1$ and muscarinic M$_2$/M$_4$ receptors was analysed in the NBM (Figure S3a,e), hippocampus (Figure S3b–d,f,g) and the cortex (Figure 3). The lesion selectively reduced M$_2$/M$_4$ receptor activity in Layers III–IV of the cortex (Figure 3a,c), with no observed effects in the NBM or hippocampus (Figure S3a–d). Conversely, low doses of WIN55,212-2 increased CB$_1$ receptor activity in lesioned animals in the same cortical layers (Figure 3b,c).

3.5 | WIN55,212-2 modified cortical acetylcholinesterase activity, acetylcholine and choline levels

We measured AChE activity, as well as ACh and choline levels in the cortex in all the experimental groups. AChE activity in the cortex decreased after the lesion (Figure 4a,b). Unexpectedly, both low and high doses of WIN55,212-2, as well as SR141716A,
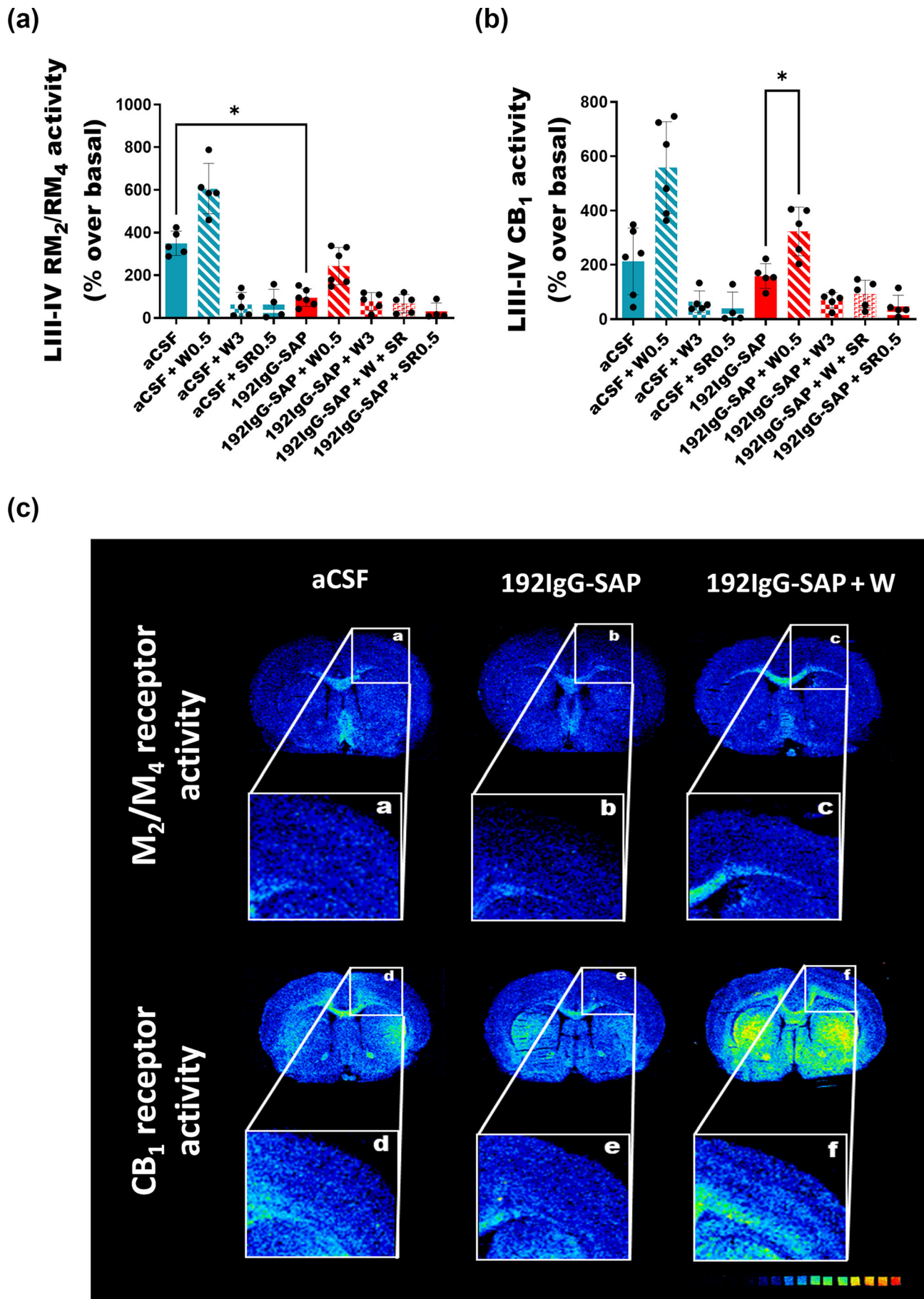
FIGURE 3 Legend on next page.

FIGURE 3 Functional autoradiographic studies of mAChR M_2/M_4 and CB_1 receptor in cortical areas of all the experimental groups. (a) Graph of mAChR M_2/M_4 and CB_1 receptor of all the experimental groups in Layers III–IV of the cortex. Scale bar = 4 mm. Data shown are individual values with means ± SEM. *$P < 0.05$, significantly different as indicated; Kruskal–Wallis test with post hoc test Dunn's multiple comparison; (n = 8) aCSF; (n = 7) aCSF + W0.5; (n = 6) aCSF + W3; (n = 6) aCSF + SR; (n = 8) 192IgG-SAP; (n = 7) 192IgG-SAP + W0.5; (n = 6) 192IgG-SAP + W3; (n = 6) 192IgG-SAP + W + SR; (n = 6) 192IgG-SAP + SR). (b) Representative autoradiographic images of brain coronal sections of muscarinic M_2/M_4 receptors and CB_1 receptors of aCSF, 192IgG-SAP and 192IgG-SAP + W0.5. Note that 192IgG-SAP + W0.5 group has same activity levels of M_2/M_4 receptors and CB_1 receptors as the aCSF group.

reversed the down-regulation of AChE activity induced by the toxin (Figure 4a,b). Cortical levels of free choline were increased in the aCSF + W0.5 groups (aCSF: 721 ± 21 vs. aCSF + W0.5: 798 ± 23. Figure 4c) compared with the aCSF group. Additionally, cortical ACh levels showed a tendency to increase in the 192IgG-SAP + W0.5 group, but a significant increase was observed in the 192IgG-SAP + W3 group compared to 192IgG-SAP (Figure 4d).

3.6 | WIN55,212-2 modified cortical lipid homeostasis

Cortical lipidomic analysis following WIN55,212-2 administration revealed more pronounced changes in lipid homeostasis compared to the effects of the cholinergic lesion alone (Figure 5a). After the lesion, cortical saturated and mono-unsaturated lysophosphatidylcholine (LPC) levels (e.g., LPC 16:0 + K+, LPC 18:0 + K+ and LPC 18:1 + K+) were significantly reduced. There was also a reduction in two phosphatidylcholines (PC) (PC 38:2 and PC O-38:7) and an increase in phosphatidylethanolamine (PE) (PE 38:5). Lipidomic changes in the 192IgG-SAP + W group, which displayed cognitive improvement after the lesion, revealed decreased arachidonic acid (AA) containing-phosphatidylcholines (PC) and phosphatidylethanolamines (PE) (e.g., PC 18:1_20:4 + K+, PC 16:0_20:4 + K+, PE 18:0_20:4 + H+, PE 18:1_20:4 + K+) and increased docosahexaenoic acid-containing phosphatidylcholines (DHA-PC), (e.g., PC 40:7 (18:1_22:6) + K + and PC 40:6 (18:0_22:6) + K+). In addition, low doses of WIN55212-2 increased very long-chain sulfatides (e.g., SHexCer (d18:1_22:0)-, SHexCer (d18:1_24:1)-) and hexoceramides (HexCer 36:1 + K+) and decreased sphingomyelins (e.g., sphingomyelin 36:1 + K+, sphingomyelin 36:2 + K+, sphingomyelin 38:1 + K+, sphingomyelin 38:2 + K+). Furthermore, low doses of WIN55212-2 increased LPCs to control levels. Interestingly, LPCs were the only lipids that correlated with behavioural parameters following BM testing in the aCSF, 192IgG-SAP, 192IgG-SAP+W and 192IgG-SAP+W + SR groups (Figure 5b). We found negative correlations with LPCs and sphingomyelins across groups (Figure 5c).

3.7 | In vitro breakdown of cortical sphingomyelins leads to increased levels of choline and LPCs

A progressive decrease of some sphingomyelins and increased levels of lysophosphatidylcholines (LPCs) were found (Figure 6a), as well as an increase in choline levels (Figure 6b). Notably, incubation of cortical tissue replicated the lipid changes observed in vivo after

WIN55,212-2 treatment. There was a strong correlation between ceramides/hexoceramides and choline levels, practically with a 1:1 ratio (Figure 6c,d). Degradation of sphingomyelin produces ceramide and phosphocholine, which is converted to choline (Figure 6e). Moreover, LPCs increased conversely to sphingomyelins (Figure 6c).

4 | DISCUSSION

The role that the eCB system plays in restoring cognitive impairment is an active area of research. Here we report that a low dose of the agonist WIN55,212-2 improved cognition following a lesion in the NBM in a rat model of cholinergic dysfunction in the CNS. In line with previous studies, injection of the neurotoxin into the NBM resulted in a loss of cholinergic p75^NTR neurons and produced a profound impairment of spatial, recognition and contextual memory in the BM and NORT assays , more pronounced in the long-term (Llorente-Ovejero et al., 2017; Llorente-Ovejero et al., 2021). The absence of cholinergic damage in the hippocampus after administration of toxin in the NBM implies that the memory impairment observed in both BM and NORT mainly reflects baso-cortical cholinergic damage (Llorente-Ovejero et al., 2021). Considering that the loss of this pathway is an early pathological feature of AD (Cummings & Back, 1998; Geula et al., 2021), we extended our investigation to an animal model of familial AD (Oddo, Caccamo, Shepherd, et al., 2003). However, male 3xTg-AD mice at 7 months did not show strong memory impairment in the BM. Using younger 3xTg-AD animals allowed us to assess cognitive deficits before motor difficulties emerge around 6 months, which could interfere with BM data interpretation (Garvock-de Montbrun et al., 2019). Although cognitive functions are already affected at this stage due to the onset of AD pathology in the 3xTg-AD mice (Belfiore et al., 2019; Muntsant et al., 2023), it appears that the cognitive deficits as measured by BM, are manifested later in disease progression (Webster et al., 2014). Although the basal forebrain cholinergic system is affected early in 3xTg-AD mice (Perez et al., 2011), alterations are age and gender-dependent, becoming more apparent after 13–15 months in female mice, and more pronounced in the hippocampus, as opposed to the basal forebrain cholinergic lesion model, where the lesioned area primarily innervates the cortex (Dennison et al., 2021). These differences in the pathological profile of both models might explain the divergent results obtained in the BM test. We previously reported cognitive impairment observed in this model at the same age (Llorente-Ovejero et al., 2018), using an aversive memory test, which is more emotionally demanding than the BM (Vorhees & Williams, 2024), but cannabinoids did not ameliorate the observed memory deficits. Given that the 3xTg-AD model at this age does not exhibit severe cognitive deficits in BM, we were unable
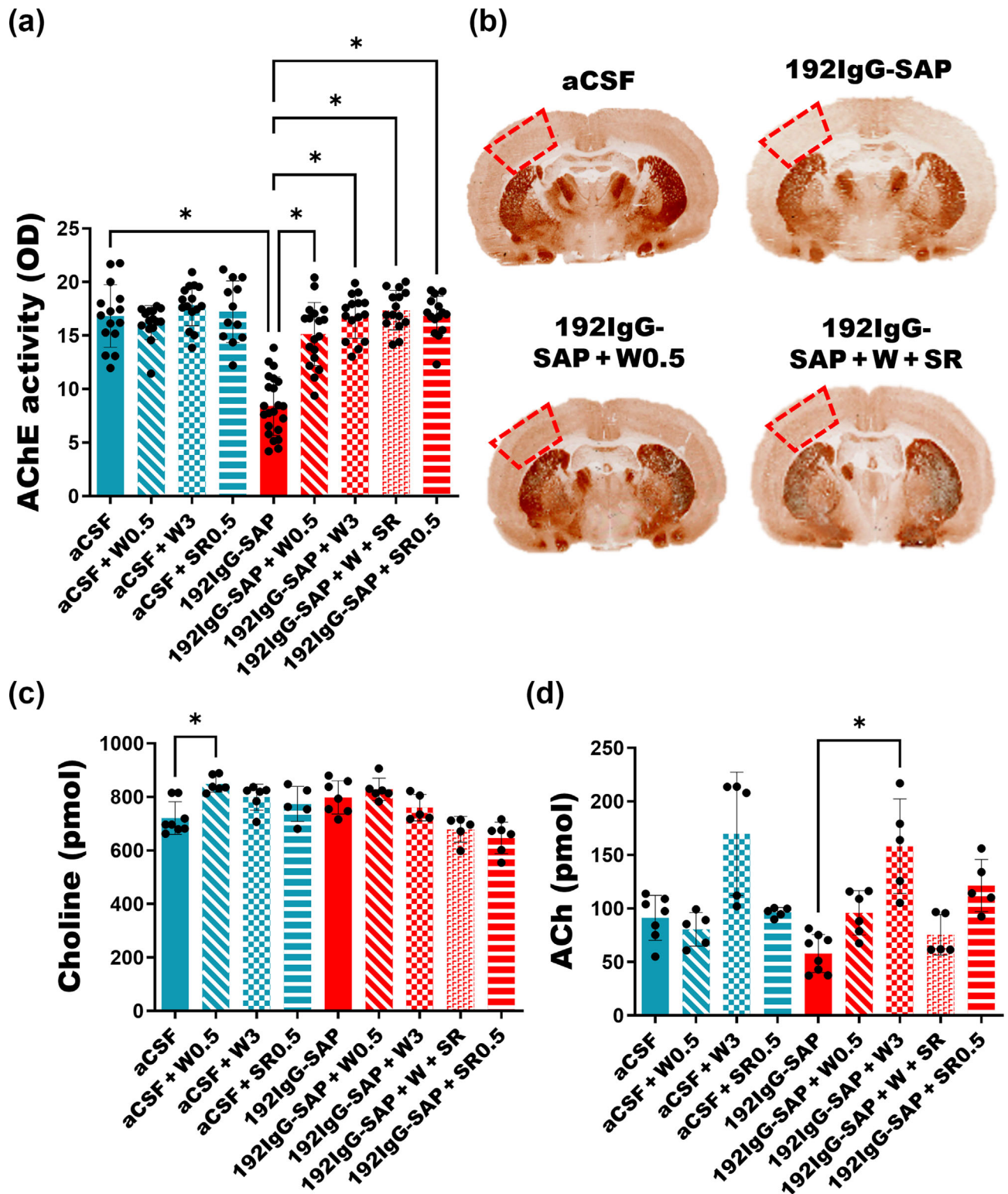
FIGURE 4 Cortical AChE activity, Ch, ACh and levels in all the experimental groups. (a) Levels of cortical AChE levels in all the experimental groups. (b) Representative images from coronal sections of AChE enzymatic staining from aCSF, 192IgG-SAP, 192IgG-SAP + W0.5 and 192IgG-SAP + W + SR groups. Note that WIN55,212-2 restores AChE cortical levels in the lesion animals. (c) Levels of cortical choline in all the experimental group. (d) Levels of cortical acetylcholine in all the experimental groups. Data shown are individual values with means ± SEM. *$P < 0.05$, significantly different as indicated; Kruskal–Wallis test with post hoc test Dunn's multiple comparison; (n = 8) aCSF; (n = 7) aCSF + W0.5; (n = 6) aCSF + W3; (n = 6) aCSF + SR; (n = 8) 192IgG-SAP; (n = 7) 192IgG-SAP + W0.5; (n = 6) 192IgG-SAP + W3; (n = 6) 192IgG-SAP + W + SR; (n = 6) 192IgG-SAP + SR.

to observe the improvements that this model could potentially offer, such as those seen in other transgenic models of AD treated with synthetic cannabinoids or enhancement of eCBs (Aso et al., 2015; Kanwal et al., 2024; Nitzan et al., 2022). Therefore, we decided to focus the study on the rat model of cholinergic dysfunction.

We did not observed a significant effect of the cannabinoid agonist on the survival of cholinergic neurons in the ex vivo model of cholinergic

degeneration, despite previous studies demonstrating the protective effect of WIN55,212-2 on cellular survival (Jeon et al., 2011; Su et al., 2015, 2016). However, in the in vivo model of BFCN degeneration, where cholinergic neurons are degenerated, the i.p. administration of a low dose (0.5 mg·kg^{-1}) of WIN55,212-2 restored cognitive impairment, as assessed by both BM and NORT. The co-administration of WIN55,212-2 with the specific CB$_1$ receptor antagonist SR141716A
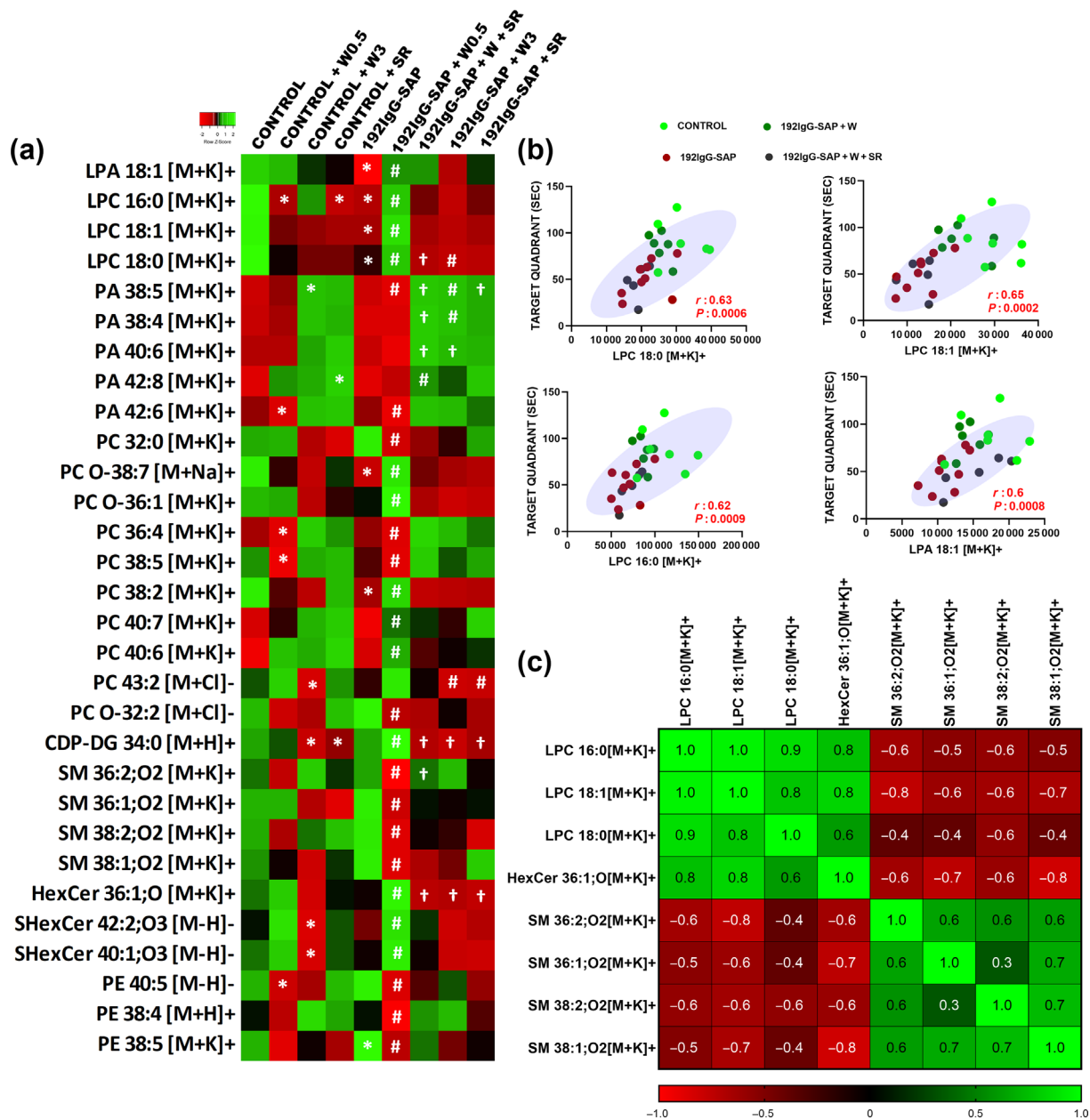

FIGURE 5 Cortical targeted lipidomic analysis. (a) Heatmap highlighting the 30 most differentially expressed lipid species between the different groups following the lesion or WIN55,212-2 treatment. *$P < 0.05$, significantly different from CONTROL; #$P < 0.05$, significantly different from 192IgG-SAP; † $P < 0.05$, significantly different from 192IgG-SAP + W0.5; Kruskal–Wallis test; post hoc test Dunn's multiple comparison; (n = 8) aCSF; (n = 7) aCSF + W0.5; (n = 6) aCSF + W3; (n = 6) aCSF + SR; (n = 8) 192IgG-SAP; (n = 7) 192IgG-SAP + W0.5; (n = 6) 192IgG-SAP + W3; (n = 6) 192IgG-SAP + W + SR; (n = 6) 192IgG-SAP + SR). (b) Linear regression showing significant correlations between LPC 18:0, LPC 18:1, LPC 16:0 and LPA 18:0, and time in target quadrant on Day 5 of Barnes maze (Spearman's rank correlation coefficient r_s and P). (c) Matrix correlation between 192IgG-SAP and 192IgG-SAP + W, showing r_s values of Spearman's correlations. Note the strong positive correlation between LPCs and HexCer, and the opposite correlation between LPC and sphingomyelins.

blocked cognitive recovery, suggesting that most of the effect was mediated by CB_1 receptors. However, as previously described by our group, there is a slight contribution of CB_2 receptors at the lesion site in this model (Llorente-Ovejero et al., 2022). Therefore, we cannot rule out the possibility that CB_2 receptors may play a role at the lesion site, particularly if the treatment exerts its positive effect through this specific area. A high dose (3 mg·kg^{-1}) of WIN55,212-2 had opposite effects depending on the treatment group, including impaired memory in controls, while improving learning in lesioned animals in the BM. Similar effects were observed in NORT with the dose of 0.5 mg·kg^{-1}. It is widely accepted that cannabinoid agonism induces memory impairment, especially short-term memory (Kohut et al., 2022; Urits et al., 2021; Zhou & Puche, 2021). Although numerous studies explore the role of cannabinoids in impairing spatial memory (Brodkin & Moerschbaecher, 1997; Ferrari et al., 1999; Hampson & Deadwyler, 1998; Hoffman et al., 2007; Varvel et al., 2001), to the best of our knowledge there have been no studies conducted with cannabinoid agonists in rats using the BM as a behavioural test. Meanwhile, earlier studies, using the NORT assay, revealed that doses of WIN55,212-2 between 0.3 and 1.2 mg·kg^{-1} are enough to completely impair short-term memory storage and different stages of long-term recognition memory (Galanopoulos et al., 2014; Schneider et al., 2008). However, there are other reports of either a biphasic effect of cannabinoid agonism on cognition (Calabrese & Rubio-Casillas, 2018), or a beneficial effects of low, as opposed to high, doses (Nitzan et al., 2022; Sarne, 2019). These results suggest that the dual effects of cannabinoids on cognition depend on several factors, for example, the state of the baso-cortical cholinergic pathway, or, more generally, the previous cognitive status of the subjects (Bilkei-Gorzo et al., 2017). This may explain why the treatment did not yield the expected positive results in 3xTg-AD mice. Significant cholinergic damage, as demonstrated by the loss of BFCN, may be necessary for WIN55,212-2 administration to be effective.

The loss of the BFCN led to an increase in Iba1-positive cells (microglia) in the region containing the NBM, as previously described following administration of 192IgG-saporin (Llorente-Ovejero et al., 2022; Seeger et al., 1997). While several studies show that cannabinoid administration reduces inflammatory activity of microglia in vitro (Facchinetti et al., 2003; Rock et al., 2007; Young & Denovan-Wright, 2022), no significant anti-inflammatory effect was observed following WIN55,212-2 administration with the dose and treatment protocol used in the present animal model. This was confirmed by lipidomic analysis, which revealed an increase in certain lipids related to microglial activation within the lesion site in the 192IgG group (Blank et al., 2022). However, after WIN55,212-2 administration, lipid levels did not decrease to control levels, indicating that WIN55,212-2 did not alter either the number or the phenotype of microglial cells at the lesion site. We previously reported an up-regulation of CB_1 receptor activity in the cortex and NBM 1 week after the lesion (Llorente-Ovejero et al., 2017). Conversely, our current findings indicate that 2 weeks after the lesion, there were no changes in CB_1 receptor activity due to the lesion in any area. A comparable progression of the eCB system response has been reported in the early stages of dementia patients, showing an increase in the initial stages followed by a decrease in the later ones (Manuel et al., 2014; Moreno-

Rodriguez et al., 2024). While cortical CB_1 and muscarinic receptor and AChE activity increased after WIN55,212-2 treatment in the lesioned animals, no changes occurred at the lesion site. This suggests that the cortex is capable of exhibiting a compensatory response similar to the up-regulation of cholinergic activity reported in the cortex of elderly individuals with mild cognitive impairment, which can be activated by cannabinoids (DeKosky et al., 2002; Ikonomovic et al., 2003; Moreno-Rodriguez et al., 2024). Taken together, these findings suggest that continuous stimulation of cortical CB_1 receptors, emulating the initial response to CB_1 receptor activation following cholinergic damage, could sustain cholinergic neurotransmission despite damage to the baso-cortical pathway.

Several earlier studies have shown that cannabinoids modulate ACh release in the hippocampus and cortex (Gessa et al., 1998; Murillo-Rodriguez et al., 2018; Nava et al., 2001; Tzavara et al., 2003). However, the specific mechanisms underlying these effects remain incompletely understood. Here, we demonstrated that, despite the loss of the majority of BFCNs, WIN55,212-2 increased cortical ACh levels while maintaining levels of choline. Conversely, in control animals, only cortical free choline increased. WIN55,212-2 appears to induce choline production, which, under conditions of cholinergic deficit, may be converted into A-Ch. Choline-containing lipids, such as phosphatidylcholines (PC), lysophosphatidylcholine (LPC) and sphingomyelins are a major source of choline (Loft et al., 2022; Okudaira et al., 2010). Besides, the generation of ACh through PC decomposition has been described (Blusztajn et al., 1987). However, the only alteration observed in cortical lipids after the lesion was a reduction in LPC levels, while CB_1 receptor activation was restored to control levels. Our group had previously reported an increase in the production of these same LPCs with the activation of muscarinic receptors (Llorente-Ovejero et al., 2021), directly connecting cholinergic signalling with LPC levels. The positive correlation observed with the cognitive status of animals in the BM assay suggests their pivotal role in maintaining cognitive function, and they are under investigation for their potential as cognitive enhancers (Tayebati & Amenta, 2013). Interestingly, SR141716A affects cortical acetylcholine levels and AChE activity similarly to WIN55,212-2 administration, as previously reported (Davis & Nomikos, 2008; Degroot et al., 2006). However, SR141716A did not produce the same behavioural improvements as WIN55,212-2, suggesting that other factors are crucial for cognitive improvement after cholinergic lesions. The specific choline-containing lipid changes induced only by low doses of WIN55,212-2 and antagonised by SR141716A along with their correlation with behavioural outcomes, strongly suggests that both the restoration of cortical cholinergic tone and the recovery of cortical choline-containing lipids are essential for memory improvement. After WIN5,212-2 administration, other choline-containing lipids, such as sphingomyelins, were markedly decreased in the cortex, which negatively correlated with LPCs. These lipids do not share a common metabolic pathway; however, both are choline-containing lipids that could serve as a potential source of choline to produce ACh. Surprisingly, the in vitro assay revealed an increase in choline levels accompanied by elevated levels of LPCs and Cer/HexCer, as well as a decrease in sphingomyelins, with a strong correlation observed between choline and Cer/HexCer. The increase in choline observed in vitro may result from the breakdown of sphingomyelins by the activation of sphingomyelinases, which
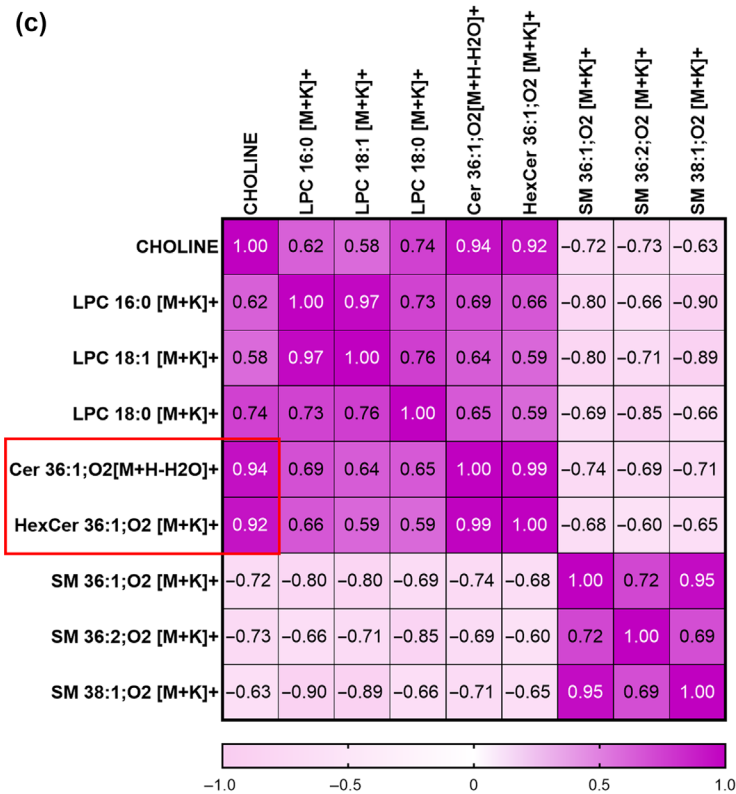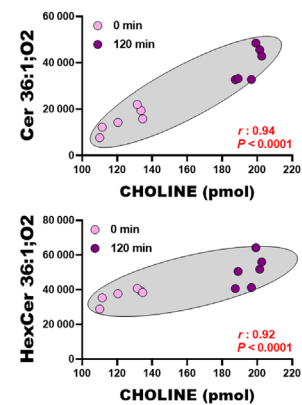
(a)
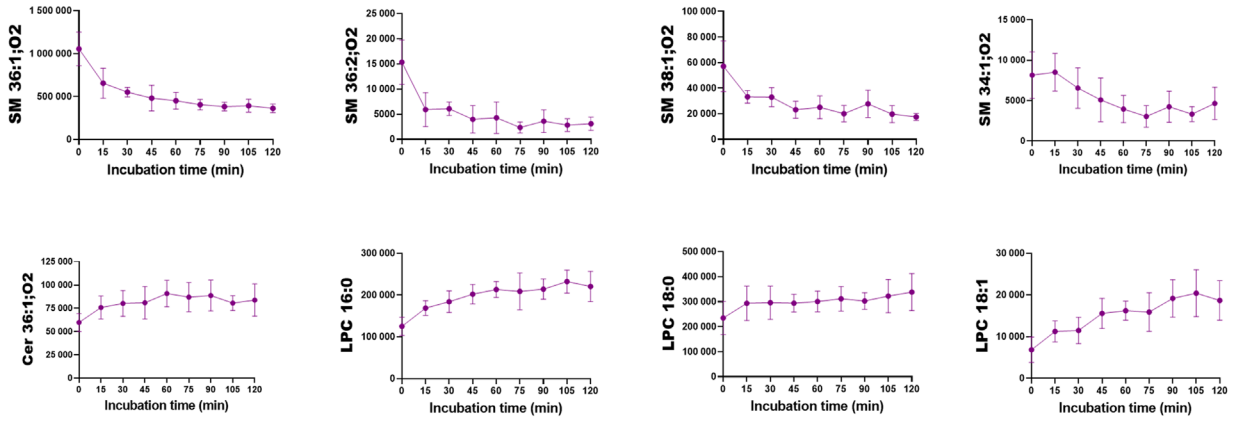
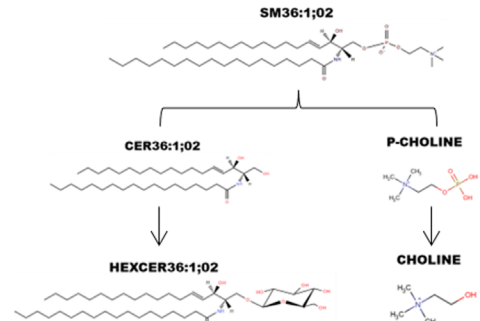**(b)**
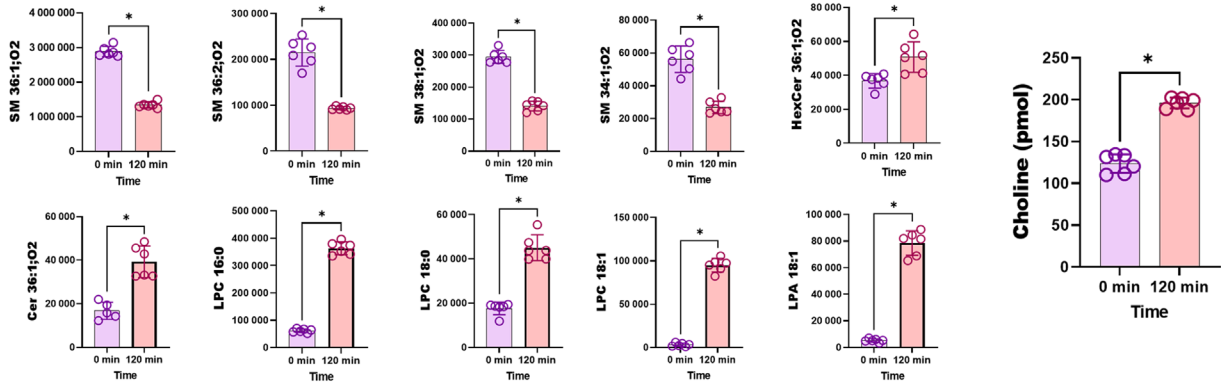
(c)

(d)

(e)

FIGURE 6 Legend on next page.

FIGURE 6 Choline production in brain cortex homogenates from control rats. (a) Line graphs of lipid production (LPCs) or degradation (sphingomyelins; SM) or ceramide (Cer) in rat brain cortex homogenates over time (n = 8, each time). (b) Changes in levels of cortical lipids and choline after 2 h of incubation. Data shown are individual values with means ± SEM; n = 6. *$P < 0.05$, significantly different as indicated; Mann–Whitney test. (c) Correlation matrix between the LPCs, sphingomyelins and choline, showing r_s values of Spearman's correlations, n = 6. Note that choline and Cer/HexCer showed strong positive correlation. (d) Linear regression shows significant correlations between Cer/HexCer and choline levels at time 0 and 120 min (Spearman's rank correlation coefficient r_s and $P < 0.05$). (e) Degradation of sphingomyelins. Degradation of sphingomyelins generates ceramide and phospho-choline. Glycosylation of ceramide generates HexCer and dephosphorylation of phospho-choline generates choline. Note that the same sphingomyelins and LPCs, whose levels are modulated by WIN55,212-2 in the cortex of lesioned rats, changed after incubation over time.

transform sphingomyelin into ceramide by cleaving the phosphocholine group (Ong et al., 2015). We demonstrate for the first time in vitro that choline can be generated by the breakdown of sphingomyelin. In addition, previous studies had shown that cannabinoids can produce ceramide through the degradation of sphingomyelins from astrocytes and tumour cells (Gomez del Pulgar et al., 2002; Guzman et al., 2001; Vijayaraghavan et al., 2024). If ceramide is produced, it also means that phosphocholine, the other component of the sphingomyelin molecule, is generated. This is supported by the finding that sphingomyelins, which decreased in vivo after WIN administration, are predominantly present in astrocytic membranes (Martínez-Gardeazabal et al., 2024). Collectively, although more research is needed on this pathway in vivo, we hypothesise that, following BFCN degeneration, WIN55,212-2, through continuous activation of CB_1 receptors in the cortex (possibly in astrocytes), triggers sphingomyelinase activation. This process leads to the generation of ceramide and free choline, which may contribute to increased ACh levels, thereby restoring cortical cholinergic neurotransmission and potentially improving memory.

While this study significantly advances our understanding of cannabinoid agonism in cholinergic lesions and memory, several limitations must be considered when interpreting the results. First, the role of CB_2 receptors was not thoroughly investigated, and their potential contributions to the observed effects remain unclear. Additionally, there is a challenge of correlating behavioural outcomes with tissue analyses, especially given the limitations of autoradiographic methods. Thus, although the study indicates that WIN55,212-2 modified choline-containing lipids and cholinergic neurotransmission, leading to restoration of memory impairment, the exact molecular mechanisms through which cannabinoid receptors mediate these effects require further research for full elucidation. Despite these limitations, this study showed that pharmacological modulation of the eCB system could be a promising therapy for neurodegenerative disorders associated with basal forebrain cholinergic degeneration.

AUTHOR CONTRIBUTIONS

Marta Moreno-Rodríguez and Rafael Rodríguez-Puertas conceived and designed the study, performed the statistical analysis, and wrote the manuscript. Alberto Llorente-Ovejero and Laura Lombardero contributed to organotypic cultures studies, such as developing an ex vivo model of cholinergic lesion and in vitro treatments. Jonatan Martínez-Gardeazabal, Marta Moreno-Rodríguez and Estibaliz González de San Román contributed to the performance of MALDI-MSI experimental procedures and data analysis. Marta Moreno-Rodríguez, Jonatan Martínez-Gardeazabal and Iker Bengoetxea de Tena performed the in vivo studies, such as surgeries, treatments and behavioural tests. Marta Moreno-Rodríguez, Jonatan Martínez-Gardeazabal and Iván Manuel performed autoradiographic studies. Marta Moreno-Rodríguez performed acetylcholinesterase activity, acetylcholine and choline assays. Marta Moreno-Rodríguez and Jonatan Martínez-Gardeazabal performed the lipidomic analysis in incubated and non-incubated samples by MALDI. All authors contributed to the manuscript revision, read and approved the submitted version.

CONFLICT OF INTEREST STATEMENT

The authors declare that the following Spanish patent related to the present work has been registered: *Tratamiento de la demencia con agonistas cannabinoides. Spain. 02-03-2017. University of the Basque Country. ES2638057.*

DATA AVAILABILITY STATEMENT

The data that support the findings of this study are available from the corresponding author upon reasonable request. Some data may not be made available because of privacy or ethical restrictions.

DECLARATION OF TRANSPARENCY AND SCIENTIFIC RIGOUR

This Declaration acknowledges that this paper adheres to the principles for transparent reporting and scientific rigour of preclinical research as stated in the *BJP* guidelines for Natural Products

Research, Design and Analysis, Immunoblotting and Immunochemistry and Animal Experimentation, and as recommended by funding agencies, publishers and other organisations engaged with supporting research.

ORCID

Marta Moreno-Rodríguez https://orcid.org/0000-0002-9980-9365

Jonatan Martínez-Gardeazabal https://orcid.org/0000-0002-0701-9076

Iker Bengoetxea de Tena https://orcid.org/0000-0003-0586-1857

Alberto Llorente-Ovejero https://orcid.org/0000-0001-8536-197X

Estibaliz González de San Román https://orcid.org/0000-0001-5440-2695

Iván Manuel https://orcid.org/0000-0003-0958-4738

Rafael Rodríguez-Puertas https://orcid.org/0000-0003-4517-5114

REFERENCES

Alexander, S. P. H., Christopoulos, A., Davenport, A. P., Kelly, E., Mathie, A. A., Peters, J. A., Veale, E. L., Armstrong, J. F., Faccenda, E., Harding, S. D., & Davies, J. A. (2023). The concise guide to PHARMACOLOGY 2023/24: G protein-coupled receptors. *British Journal of Pharmacology*, 180(Suppl 2), S23–S144.

Alexander, S. P. H., Fabbro, D., Kelly, E., Mathie, A. A., Peters, J. A., Veale, E. L., Armstrong, J. F., Faccenda, E., Harding, S. D., Davies, J. A., Annett, S., Boison, D., Burns, K. E., Dessauer, C., Gertsch, J., Helsby, N. A., Izzo, A. A., Ostrom, R., Papapetropoulos, A., … Wong, S. S. (2023). The Concise Guide to PHARMACOLOGY 2023/24: Enzymes. *British Journal of Pharmacology*, 180(Suppl 2), S289–S373. https://doi.org/10.1111/bph.16181

Alexander, S. P. H., Roberts, R. E., Broughton, B. R. S., Sobey, C. G., George, C. H., Stanford, S. C., Docherty, J. R., Giembycz, M. A., Hoyer, D., Insel, P. A., Izzo, A. A., Ji, Y., MacEwan, D. J., Mangum, J., Wonnacott, S., & Ahluwalia, A. (2018). Goals and practicalities of immunoblotting and immunohistochemistry: A guide for submission to the British Journal of pharmacology. *British Journal of Pharmacology*, 175, 407–411. https://doi.org/10.1111/bph.14112

Aso, E., Sanchez-Pla, A., Vegas-Lozano, E., Maldonado, R., & Ferrer, I. (2015). Cannabis-based medicine reduces multiple pathological processes in AbetaPP/PS1 mice. *Journal of Alzheimer's Disease*, 43, 977–991. https://doi.org/10.3233/JAD-141014

Belfiore, R., Rodin, A., Ferreira, E., Velazquez, R., Branca, C., Caccamo, A., & Oddo, S. (2019). Temporal and regional progression of Alzheimer's disease-like pathology in 3xTg-AD mice. *Aging Cell*, 18, e12873. https://doi.org/10.1111/acel.12873

Benito, C., Nunez, E., Tolon, R. M., Carrier, E. J., Rabano, A., Hillard, C. J., & Romero, J. (2003). Cannabinoid CB2 receptors and fatty acid amide hydrolase are selectively overexpressed in neuritic plaque-associated glia in Alzheimer's disease brains. *The Journal of Neuroscience*, 23, 11136–11141. https://doi.org/10.1523/JNEUROSCI.23-35-11136.2003

Bengoetxea de Tena, I., Moreno-Rodríguez, M., Llorente-Ovejero, A., Monge-Benito, S., Martínez-Gardeazabal, J., Onandia-Hinchado, I., Manuel, I., Giménez-Llort, L., & Rodríguez-Puertas, R. (2022). Handling and novel object recognition modulate fear response and endocannabinoid signaling in nucleus basalis magnocellularis. *European Journal of Neuroscience*, 55, 1532-1546. https://doi.org/10.1111/ejn.15642

Bilkei-Gorzo, A., Albayram, O., Draffehn, A., Michel, K., Piyanova, A., Oppenheimer, H., Dvir-Ginzberg, M., Rácz, I., Ulas, T., Imbeault, S., Bab, I., Schultze, J. L., & Zimmer, A. (2017). A chronic low dose of Delta(9)-tetrahydrocannabinol (THC) restores cognitive function in old mice. *Nature Medicine*, 23, 782–787. https://doi.org/10.1038/nm.4311

Blank, M., Enzlein, T., & Hopf, C. (2022). LPS-induced lipid alterations in microglia revealed by MALDI mass spectrometry-based cell fingerprinting in neuroinflammation studies. *Scientific Reports*, 12, 2908. https://doi.org/10.1038/s41598-022-06894-1

Blusztajn, J. K., Liscovitch, M., & Richardson, U. I. (1987). Synthesis of acetylcholine from choline derived from phosphatidylcholine in a human neuronal cell line. *Proceedings of the National Academy of Sciences of the United States of America*, 84, 5474–5477. https://doi.org/10.1073/pnas.84.15.5474

Blusztajn, J. K., & Wurtman, R. J. (1983). Choline and cholinergic neurons. *Science*, 221, 614–620. https://doi.org/10.1126/science.6867732

Brodkin, J., & Moerschbaecher, J. M. (1997). SR141716A antagonizes the disruptive effects of cannabinoid ligands on learning in rats. *The Journal of Pharmacology and Experimental Therapeutics*, 282, 1526–1532.

Broyd, S. J., van Hell, H. H., Beale, C., Yucel, M., & Solowij, N. (2016). Acute and chronic effects of cannabinoids on human cognition-a systematic review. *Biological Psychiatry*, 79, 557–567. https://doi.org/10.1016/j.biopsych.2015.12.002

Calabrese, E. J., & Rubio-Casillas, A. (2018). Biphasic effects of THC in memory and cognition. *European Journal of Clinical Investigation*, 48, e12920. https://doi.org/10.1111/eci.12920

Cummings, J. L., & Back, C. (1998). The cholinergic hypothesis of neuropsychiatric symptoms in Alzheimer's disease. *The American Journal of Geriatric Psychiatry*, 6, S64–S78. https://doi.org/10.1097/00019442-199821001-00009

Curtis, M. J., Alexander, S. P. H., Cirino, G., George, C. H., Kendall, D. A., Insel, P. A., Izzo, A. A., Ji, Y., Panettieri, R. A., Patel, H. H., Sobey, C. G., Stanford, S. C., Stanley, P., Stefanska, B., Stephens, G. J., Teixeira, M. M., Vergnolle, N., & Ahluwalia, A. (2022). Planning experiments: Updated guidance on experimental design and analysis and their reporting III. *British Journal of Pharmacology*, 179, 3907–3913. https://doi.org/10.1111/bph.15868

Davis, R. J., & Nomikos, G. G. (2008). Oral administration of the antiobesity drugs, sibutramine and rimonabant, increases acetylcholine efflux selectively in the medial prefrontal cortex of the rat. *Molecular Psychiatry*, 13, 240–241. https://doi.org/10.1038/sj.mp.4002112

Degroot, A., Kofalvi, A., Wade, M. R., Davis, R. J., Rodrigues, R. J., Rebola, N., Cunha, R. A., & Nomikos, G. G. (2006). CB1 receptor antagonism increases hippocampal acetylcholine release: Site and mechanism of action. *Molecular Pharmacology*, 70, 1236–1245. https://doi.org/10.1124/mol.106.024661

DeKosky, S. T., Ikonomovic, M. D., Styren, S. D., Beckett, L., Wisniewski, S., Bennett, D. A., Cochran, E. J., Kordower, J. H., & Mufson, E. J. (2002). Upregulation of choline acetyltransferase activity in hippocampus and frontal cortex of elderly subjects with mild cognitive impairment. *Annals of Neurology*, 51, 145–155. https://doi.org/10.1002/ana.10069

Dennison, J. L., Ricciardi, N. R., Lohse, I., Volmar, C. H., & Wahlestedt, C. (2021). Sexual dimorphism in the 3xTg-AD mouse model and its impact on pre-clinical research. *Journal of Alzheimer's Disease*, 80, 41–52. https://doi.org/10.3233/JAD-201014

Facchinetti, F., Del Giudice, E., Furegato, S., Passarotto, M., & Leon, A. (2003). Cannabinoids ablate release of TNFalpha in rat microglial cells stimulated with lypopolysaccharide. *Glia*, 41, 161–168. https://doi.org/10.1002/glia.10177

Fernandez-Moncada, I., Eraso-Pichot, A., Dalla Tor, T., Fortunato-Marsol, B., & Marsicano, G. (2023). An enquiry to the role of CB1 receptors in neurodegeneration. *Neurobiology of Disease*, 184, 106235. https://doi.org/10.1016/j.nbd.2023.106235

Ferrari, F., Ottani, A., Vivoli, R., & Giuliani, D. (1999). Learning impairment produced in rats by the cannabinoid agonist HU 210 in a water-maze task. *Pharmacology, Biochemistry, and Behavior*, 64, 555–561. https://doi.org/10.1016/S0091-3057(99)00106-9

Galanopoulos, A., Polissidis, A., Georgiadou, G., Papadopoulou-Daifoti, Z., Nomikos, G. G., Pitsikas, N., & Antoniou, K. (2014). WIN55,212-2

impairs non-associative recognition and spatial memory in rats via CB1 receptor stimulation. *Pharmacology, Biochemistry, and Behavior*, *124*, 58–66. https://doi.org/10.1016/j.pbb.2014.05.014

Garvock-de Montbrun, T., Fertan, E., Stover, K., & Brown, R. E. (2019). Motor deficits in 16-month-old male and female 3xTg-AD mice. *Behavioural Brain Research*, *356*, 305–313. https://doi.org/10.1016/j.bbr.2018.09.006

Gessa, G. L., Casu, M. A., Carta, G., & Mascia, M. S. (1998). Cannabinoids decrease acetylcholine release in the medial-prefrontal cortex and hippocampus, reversal by SR 141716A. *European Journal of Pharmacology*, *355*, 119–124. https://doi.org/10.1016/S0014-2999(98)00486-5

Gessa, G. L., Mascia, M. S., Casu, M. A., & Carta, G. (1997). Inhibition of hippocampal acetylcholine release by cannabinoids: Reversal by SR 141716A. *European Journal of Pharmacology*, *327*, R1–R2. https://doi.org/10.1016/S0014-2999(97)89683-5

Geula, C., Dunlop, S. R., Ayala, I., Kawles, A. S., Flanagan, M. E., Gefen, T., & Mesulam, M. M. (2021). Basal forebrain cholinergic system in the dementias: Vulnerability, resilience, and resistance. *Journal of Neurochemistry*, *158*, 1394–1411. https://doi.org/10.1111/jnc.15471

Gomez del Pulgar, T., Velasco, G., Sanchez, C., Haro, A., & Guzman, M. (2002). De novo-synthesized ceramide is involved in cannabinoid-induced apoptosis. *The Biochemical Journal*, *363*, 183–188. https://doi.org/10.1042/bj3630183

Goonawardena, A. V., Robinson, L., Hampson, R. E., & Riedel, G. (2010). Cannabinoid and cholinergic systems interact during performance of a short-term memory task in the rat. *Learning & Memory*, *17*, 502–511. https://doi.org/10.1101/lm.1893710

Grothe, M., Heinsen, H., & Teipel, S. (2013). Longitudinal measures of cholinergic forebrain atrophy in the transition from healthy aging to Alzheimer's disease. *Neurobiology of Aging*, *34*, 1210–1220. https://doi.org/10.1016/j.neurobiolaging.2012.10.018

Grothe, M., Heinsen, H., & Teipel, S. J. (2012). Atrophy of the cholinergic basal forebrain over the adult age range and in early stages of Alzheimer's disease. *Biological Psychiatry*, *71*, 805–813. https://doi.org/10.1016/j.biopsych.2011.06.019

Guzman, M., Galve-Roperh, I., & Sanchez, C. (2001). Ceramide: A new second messenger of cannabinoid action. *Trends in Pharmacological Sciences*, *22*, 19–22. https://doi.org/10.1016/S0165-6147(00)01586-8

Hampson, R. E., & Deadwyler, S. A. (1998). Role of cannabinoid receptors in memory storage. *Neurobiology of Disease*, *5*, 474–482. https://doi.org/10.1006/nbdi.1998.0223

Harkany, T., Hartig, W., Berghuis, P., Dobszay, M. B., Zilberter, Y., Edwards, R. H., Mackie, K., & Ernfors, P. (2003). Complementary distribution of type 1 cannabinoid receptors and vesicular glutamate transporter 3 in basal forebrain suggests input-specific retrograde signalling by cholinergic neurons. *The European Journal of Neuroscience*, *18*, 1979–1992. https://doi.org/10.1046/j.1460-9568.2003.02898.x

Hoffman, A. F., Oz, M., Yang, R., Lichtman, A. H., & Lupica, C. R. (2007). Opposing actions of chronic Delta9-tetrahydrocannabinol and cannabinoid antagonists on hippocampal long-term potentiation. *Learning & Memory*, *14*, 63–74. https://doi.org/10.1101/lm.439007

Ikonomovic, M. D., Mufson, E. J., Wuu, J., Cochran, E. J., Bennett, D. A., & DeKosky, S. T. (2003). Cholinergic plasticity in hippocampus of individuals with mild cognitive impairment: Correlation with Alzheimer's neuropathology. *Journal of Alzheimer's Disease: JAD*, *5*, 39–48. https://doi.org/10.3233/JAD-2003-5106

Jeon, P., Yang, S., Jeong, H., & Kim, H. (2011). Cannabinoid receptor agonist protects cultured dopaminergic neurons from the death by the proteasomal dysfunction. *Anatomy & Cell Biology*, *44*, 135–142. https://doi.org/10.5115/acb.2011.44.2.135

Kanwal, H., Sangineto, M., Ciarnelli, M., Castaldo, P., Villani, R., Romano, A. D., Serviddio, G., & Cassano, T. (2024). Potential therapeutic targets to modulate the endocannabinoid system in Alzheimer's Disease. *International Journal of Molecular Sciences*, *25*, 4050. https://doi.org/10.3390/ijms25074050

Koch, M., Kreutz, S., Bottger, C., Grabiec, U., Ghadban, C., Korf, H. W., & Dehghani, F. (2011). The cannabinoid WIN 55,212-2-mediated protection of dentate gyrus granule cells is driven by CB1 receptors and modulated by TRPA1 and Cav 2.2 channels. *Hippocampus*, *21*, 554–564. https://doi.org/10.1002/hipo.20772

Kohut, S. J., Cao, L., Mintzopoulous, D., Jiang, S., Nikas, S. P., Makriyannis, A., Zou, C. S., Jensen, J. E., Frederick, B. B., Bergman, J., & Kangas, B. D. (2022). Effects of cannabinoid exposure on short-term memory and medial orbitofrontal cortex function and chemistry in adolescent female rhesus macaques. *Frontiers in Neuroscience*, *16*, 998351. https://doi.org/10.3389/fnins.2022.998351

Lee, J. H., Agacinski, G., Williams, J. H., Wilcock, G. K., Esiri, M. M., Francis, P. T., Wong, P. T. H., Chen, C. P., & Lai, M. K. P. (2010). Intact cannabinoid CB1 receptors in the Alzheimer's disease cortex. *Neurochemistry International*, *57*, 985–989. https://doi.org/10.1016/j.neuint.2010.10.010

Lilley, E., Stanford, S. C., Kendall, D. E., Alexander, S. P. H., Cirino, G., Docherty, J. R., George, C. H., Insel, P. A., Izzo, A. A., Ji, Y., Panettieri, R. A., Sobey, C. G., Stefanska, B., Stephens, G., Teixeira, M. M., & Ahluwalia, A. (2020). ARRIVE 2.0 and the British Journal of Pharmacology: Updated guidance for 2020. *British Journal of Pharmacology*, *177*, 3611–3616. https://doi.org/10.1111/bph.15178

Llorente-Ovejero, A., Bengoetxea de Tena, I., Martinez-Gardeazabal, J., Moreno-Rodriguez, M., Lombardero, L., Manuel, I., & Rodríguez-Puertas, R. (2022). Cannabinoid receptors and glial response following a basal forebrain cholinergic lesion. *ACS Pharmacology & Translational Science*, *5*, 791–802. https://doi.org/10.1021/acsptsci.2c00069

Llorente-Ovejero, A., Manuel, I., Giralt, M. T., & Rodriguez-Puertas, R. (2017). Increase in cortical endocannabinoid signaling in a rat model of basal forebrain cholinergic dysfunction. *Neuroscience*, *362*, 206–218. https://doi.org/10.1016/j.neuroscience.2017.08.008

Llorente-Ovejero, A., Manuel, I., Lombardero, L., Giralt, M. T., Ledent, C., Gimenez-Llort, L., & Rodríguez-Puertas, R. (2018). Endocannabinoid and muscarinic signaling crosstalk in the 3xTg-AD mouse model of Alzheimer's Disease. *Journal of Alzheimer's Disease: JAD*, *64*, 117–136. https://doi.org/10.3233/JAD-180137

Llorente-Ovejero, A., Martinez-Gardeazabal, J., Moreno-Rodriguez, M., Lombardero, L., de San, G., Roman, E., Manuel, I., Giralt, M. T., & Rodríguez-Puertas, R. (2021). Specific phospholipid modulation by muscarinic signaling in a rat lesion model of Alzheimer's Disease. *ACS Chemical Neuroscience*, *12*, 2167–2181. https://doi.org/10.1021/acschemneuro.1c00169

Loft, L. M. I., Moseholm, K. F., Pedersen, K. K. W., Jensen, M. K., Koch, M., & Cronje, H. T. (2022). Sphingomyelins and ceramides: Possible biomarkers for dementia? *Current Opinion in Lipidology*, *33*, 57–67. https://doi.org/10.1097/MOL.0000000000000804

Manuel, I., de San, G., Roman, E., Giralt, M. T., Ferrer, I., & Rodriguez-Puertas, R. (2014). Type-1 cannabinoid receptor activity during Alzheimer's disease progression. *Journal of Alzheimer's Disease: JAD*, *42*, 761–766. https://doi.org/10.3233/JAD-140492

Martinez-Gardeazabal, J., Moreno-Rodriguez, M., de San Roman, E. G., Abad, B., Manuel, I., & Rodriguez-Puertas, R. (2023). Mass spectrometry for the advancement of lipid analysis in Alzheimer's research. *Methods in Molecular Biology*, *2561*, 245–259. https://doi.org/10.1007/978-1-0716-2655-9_13

Martínez-Gardeazabal, J., Moreno-Rodríguez, M., Llorente-Ovejero, A., Gonález de San Román, E., Lombardero, L., de Tena, I.B., Sustacha, J., Matute, C., Manuel, I., Bonifazi, P., & Rodríguez-Puertas, R. (2024). Cell lipotypes localization in brain by mass spectrometry imaging. https://doi.org/10.1101/2024.02.02.578599

Medina-Vera, D., Zhao, H., Bereczki, E., Rosell-Valle, C., Shimozawa, M., Chen, G., de Fonseca, F. R., Nilsson, P., & Tambaro, S. (2023). The

expression of the endocannabinoid receptors CB2 and GPR55 is highly increased during the progression of Alzheimer's Disease in app (NL-G-F) Knock-in mice. *Biology (Basel)*, 12, 805. https://doi.org/10.3390/biology12060

Moreno-Rodriguez, M., Perez, S. E., Martinez-Gardeazabal, J., Manuel, I., Malek-Ahmadi, M., Rodriguez-Puertas, R., & Mufson, E. J. (2024). Frontal cortex lipid alterations during the onset of Alzheimer's Disease. *Journal of Alzheimer's Disease*, 98, 1515–1532. https://doi.org/10.3233/JAD-231485

Moreta, M. P., Burgos-Alonso, N., Torrecilla, M., Marco-Contelles, J., & Bruzos-Cidon, C. (2021). Efficacy of acetylcholinesterase inhibitors on cognitive function in Alzheimer's Disease. Review of reviews. *Biomedicines*, 9, 1689. https://doi.org/10.3390/biomedicines9111689

Mulder, J., Zilberter, M., Pasquare, S. J., Alpar, A., Schulte, G., Ferreira, S. G., Koefalvi, A., Martin-Moreno, A. M., Keimpema, E., Tanila, H., & Watanabe, M. (2011). Molecular reorganization of endocannabinoid signalling in Alzheimer's disease. *Brain*, 134, 1041–1060. https://doi.org/10.1093/brain/awr046

Muntsant, A., Castillo-Ruiz, M. D. M., & Gimenez-Llort, L. (2023). Survival bias, non-lineal behavioral and Cortico-limbic neuropathological signatures in 3xTg-AD mice for Alzheimer's Disease from premorbid to advanced stages and compared to Normal aging. *International Journal of Molecular Sciences*, 24, 13796. https://doi.org/10.3390/ijms241813796

Murillo-Rodriguez, E., Arankowsky-Sandoval, G., Rocha, N. B., Peniche-Amante, R., Veras, A. B., Machado, S., & Budde, H. (2018). Systemic injections of Cannabidiol enhance acetylcholine levels from basal forebrain in rats. *Neurochemical Research*, 43, 1511–1518. https://doi.org/10.1007/s11064-018-2565-0

Nair, A. B., & Jacob, S. (2016). A simple practice guide for dose conversion between animals and human. *Journal of Basic and Clinical Pharmacy*, 7, 27–31. https://doi.org/10.4103/0976-0105.177703

Nava, F., Carta, G., Colombo, G., & Gessa, G. L. (2001). Effects of chronic Delta(9)-tetrahydrocannabinol treatment on hippocampal extracellular acetylcholine concentration and alternation performance in the T-maze. *Neuropharmacology*, 41, 392–399. https://doi.org/10.1016/S0028-3908(01)00075-2

Nemy, M., Dyrba, M., Brosseron, F., Buerger, K., Dechent, P., Dobisch, L., Ewers, M., Fliessbach, K., Glanz, W., Goerss, D., Heneka, M. T., Hetzer, S., Incesoy, E. I., Janowitz, D., Kilimann, I., Laske, C., Maier, F., Munk, M. H., Perneczky, R., ... Ferreira, D. (2023). Cholinergic white matter pathways along the Alzheimer's disease continuum. *Brain*, 146, 2075–2088. https://doi.org/10.1093/brain/awac385

Nitzan, K., Ellenbogen, L., Bentulila, Z., David, D., Franko, M., Break, E. P., Zoharetz, M., Shamir, A., Sarne, Y., & Doron, R. (2022). An ultra-low dose of Δ9-tetrahydrocannabinol alleviates Alzheimer's Disease-related cognitive impairments and modulates TrkB receptor expression in a 5XFAD mouse model. *International Journal of Molecular Sciences*, 23, 9449. https://doi.org/10.3390/ijms23169449

Oddo, S., Caccamo, A., Kitazawa, M., Tseng, B. P., & LaFerla, F. M. (2003). Amyloid deposition precedes tangle formation in a triple transgenic model of Alzheimer's disease. *Neurobiology of Aging*, 24, 1063–1070. https://doi.org/10.1016/j.neurobiolaging.2003.08.012

Oddo, S., Caccamo, A., Shepherd, J. D., Murphy, M. P., Golde, T. E., Kayed, R., Metherate, R., Mattson, M. P., Akbari, Y., & LaFerla, F. M. (2003). Triple-transgenic model of Alzheimer's disease with plaques and tangles: Intracellular Abeta and synaptic dysfunction. *Neuron*, 39, 409–421. https://doi.org/10.1016/S0896-6273(03)00434-3

Okudaira, S., Yukiura, H., & Aoki, J. (2010). Biological roles of lysophosphatidic acid signaling through its production by autotaxin. *Biochimie*, 92, 698–706. https://doi.org/10.1016/j.biochi.2010.04.015

Ong, W. Y., Herr, D. R., Farooqui, T., Ling, E. A., & Farooqui, A. A. (2015). Role of sphingomyelinases in neurological disorders. *Expert Opinion on Therapeutic Targets*, 19, 1725–1742. https://doi.org/10.1517/14728222.2015.1071794

Ozaita, A., & Aso, E. (2017). The cannabis paradox: When age matters. *Nature Medicine*, 23, 661–662. https://doi.org/10.1038/nm.4348

Percie du Sert, N., Hurst, V., Ahluwalia, A., Alam, S., Avey, M. T., Baker, M., Browne, W. J., Clark, A., Cuthill, I. C., Dirnagl, U., Emerson, M., Garner, P., Holgate, S. T., Howells, D. W., Karp, N. A., Lazic, S. E., Lidster, K., MacCallum, C. J., Macleod, M., ... Würbel, H. (2020). The ARRIVE guidelines 2.0: updated guidelines for reporting animal research. *PLoS Biol*, 18, e3000410. https://doi.org/10.1371/journal.pbio.3000410

Perez, S. E., He, B., Muhammad, N., Oh, K. J., Fahnestock, M., Ikonomovic, M. D., & Mufson, E. J. (2011). Cholinotrophic basal forebrain system alterations in 3xTg-AD transgenic mice. *Neurobiology of Disease*, 41, 338–352. https://doi.org/10.1016/j.nbd.2010.10.002

Potter, P. E., Rauschkolb, P. K., Pandya, Y., Sue, L. I., Sabbagh, M. N., Walker, D. G., & Beach, T. G. (2011). Pre- and post-synaptic cortical cholinergic deficits are proportional to amyloid plaque presence and density at preclinical stages of Alzheimer's disease. *Acta Neuropathologica*, 122, 49–60. https://doi.org/10.1007/s00401-011-0831-1

Puighermanal, E., Busquets-Garcia, A., Maldonado, R., & Ozaita, A. (2012). Cellular and intracellular mechanisms involved in the cognitive impairment of cannabinoids. *Philosophical Transactions of the Royal Society of London. Series B, Biological Sciences*, 367, 3254–3263. https://doi.org/10.1098/rstb.2011.0384

Robichaud, G., Garrard, K. P., Barry, J. A., & Muddiman, D. C. (2013). MSiReader: An open-source interface to view and analyze high resolving power MS imaging files on Matlab platform. *Journal of the American Society for Mass Spectrometry*, 24, 718–721. https://doi.org/10.1007/s13361-013-0607-z

Rock, R. B., Gekker, G., Hu, S., Sheng, W. S., Cabral, G. A., Martin, B. R., & Peterson, P. K. (2007). WIN55,212-2-mediated inhibition of HIV-1 expression in microglial cells: Involvement of cannabinoid receptors. *Journal of Neuroimmune Pharmacology*, 2, 178–183. https://doi.org/10.1007/s11481-006-9040-4

Rossner, S. (1997). Cholinergic immunolesions by 192IgG-saporin—A useful tool to simulate pathogenic aspects of alzheimer's disease. *International Journal of Developmental Neuroscience*, 15, 835–850. https://doi.org/10.1016/S0736-5748(97)00035-X

Ruiz de Martin Esteban, S., Benito-Cuesta, I., Terradillos, I., Martinez-Relimpio, A. M., Arnanz, M. A., Ruiz-Perez, G., Korn, C., Raposo, C., Sarott, R. C., Westphal, M. V., & Elezgarai, I. (2022). Cannabinoid CB(2) receptors modulate microglia function and amyloid dynamics in a mouse model of Alzheimer's Disease. *Frontiers in Pharmacology*, 13, 841766.

Ruver-Martins, A. C., Bicca, M. A., de Araujo, F. S., de Noronha Sales Maia, B. H. L., Pamplona, F. A., da Silva, E. G., & Nascimento, F. P. (2022). Cannabinoid extract in microdoses ameliorates mnemonic and nonmnemonic Alzheimer's disease symptoms: A case report. *Journal of Medical Case Reports*, 16, 277. https://doi.org/10.1186/s13256-022-03457-w

Sarne, Y. (2019). Beneficial and deleterious effects of cannabinoids in the brain: The case of ultra-low dose THC. *The American Journal of Drug and Alcohol Abuse*, 45, 551–562. https://doi.org/10.1080/00952990.2019.1578366

Schliebs, R., Rossner, S., & Bigl, V. (1996). Immunolesion by 192IgG-saporin of rat basal forebrain cholinergic system: A useful tool to produce cortical cholinergic dysfunction. *Progress in Brain Research*, 109, 253–264. https://doi.org/10.1016/S0079-6123(08)62109-3

Schneider, M., Schomig, E., & Leweke, F. M. (2008). Acute and chronic cannabinoid treatment differentially affects recognition memory and social behavior in pubertal and adult rats. *Addiction Biology*, 13, 345–357. https://doi.org/10.1111/j.1369-1600.2008.00117.x

Schumacher, J., Ray, N. J., Hamilton, C. A., Bergamino, M., Donaghy, P. C., Firbank, M., Watson, R., Roberts, G., Allan, L., Barnett, N., O'Brien, J. T., Thomas, A. J., & Taylor, J. P. (2023). Free water imaging of the cholinergic system in dementia with Lewy bodies and

Alzheimer's disease. *Alzheimers Dement*, 19, 4549–4563. https://doi.org/10.1002/alz.13034

Seeger, G., Hartig, W., Rossner, S., Schliebs, R., Bruckner, G., Bigl, V., & Brauer, K. (1997). Electron microscopic evidence for microglial phagocytic activity and cholinergic cell death after administration of the immunotoxin 192IgG-saporin in rat. *Journal of Neuroscience Research*, 48, 465–476. https://doi.org/10.1002/(SICI)1097-4547(19970601)48:5<465::AID-JNR7>3.0.CO;2-C

Shanks, H. R. C., Onuska, K. M., Barupal, D. K., Schmitz, T. W., Alzheimer's Disease Neuroimaging Initiative, & Alzheimer's Disease Metabolomics Consortium. (2022). Serum unsaturated phosphatidylcholines predict longitudinal basal forebrain degeneration in Alzheimer's disease. *Brain Communications*, 4, fcac318. https://doi.org/10.1093/braincomms/fcac318

Solas, M., Francis, P. T., Franco, R., & Ramirez, M. J. (2013). CB2 receptor and amyloid pathology in frontal cortex of Alzheimer's disease patients. *Neurobiology of Aging*, 34, 805–808. https://doi.org/10.1016/j.neurobiolaging.2012.06.005

Su, S. H., Wang, Y. Q., Wu, Y. F., Wang, D. P., Lin, Q., & Hai, J. (2016). Cannabinoid receptor agonist WIN55,212-2 and fatty acid amide hydrolase inhibitor URB597 may protect against cognitive impairment in rats of chronic cerebral hypoperfusion via PI3K/AKT signaling. *Behavioural Brain Research*, 313, 334–344. https://doi.org/10.1016/j.bbr.2016.07.009

Su, S. H., Wu, Y. F., Lin, Q., Yu, F., & Hai, J. (2015). Cannabinoid receptor agonist WIN55,212-2 and fatty acid amide hydrolase inhibitor URB597 suppress chronic cerebral hypoperfusion-induced neuronal apoptosis by inhibiting c-Jun N-terminal kinase signaling. *Neuroscience*, 301, 563–575. https://doi.org/10.1016/j.neuroscience.2015.03.021

Tayebati, S. K., & Amenta, F. (2013). Choline-containing phospholipids: Relevance to brain functional pathways. *Clinical Chemistry and Laboratory Medicine*, 51, 513–521. https://doi.org/10.1515/cclm-2012-0559

Tzavara, E. T., Wade, M., & Nomikos, G. G. (2003). Biphasic effects of cannabinoids on acetylcholine release in the hippocampus: Site and mechanism of action. *The Journal of Neuroscience: the Official Journal of the Society for Neuroscience*, 23, 9374–9384. https://doi.org/10.1523/JNEUROSCI.23-28-09374.2003

Urits, I., Charipova, K., Gress, K., Li, N., Berger, A. A., Cornett, E. M., Kassem, H., Ngo, A. L., Kaye, A. D., & Viswanath, O. (2021). Adverse effects of recreational and medical cannabis. *Psychopharmacology Bulletin*, 51, 94–109.

Varvel, S. A., Hamm, R. J., Martin, B. R., & Lichtman, A. H. (2001). Differential effects of delta 9-THC on spatial reference and working memory in mice. *Psychopharmacology*, 157, 142–150.

Vijayaraghavan, C. S., Raman, L. S., Surenderan, S., Kaur, H., Chinambedu, M. D., Thyagarajan, S. P., & Gnanambal Krishnan, M. E. (2024). A novel non-psychoactive fatty acid from a marine snail, Conus inscriptus, signals cannabinoid receptor 1 (CB1) to accumulate apoptotic C16:0 and C18:0 ceramides in Teratocarcinoma cell line PA1. *Molecules*, 29, 1737. https://doi.org/10.3390/molecules29081737

Vorhees, C. V., & Williams, M. T. (2024). Tests for learning and memory in rodent regulatory studies. *Current Research in Toxicology*, 6, 100151. https://doi.org/10.1016/j.crtox.2024.100151

Webster, S. J., Bachstetter, A. D., Nelson, P. T., Schmitt, F. A., & Van Eldik, L. J. (2014). Using mice to model Alzheimer's dementia: An overview of the clinical disease and the preclinical behavioral changes in 10 mouse models. *Frontiers in Genetics*, 5, 88.

Whitehouse, P. J., Price, D. L., Clark, A. W., Coyle, J. T., & DeLong, M. R. (1981). Alzheimer disease: Evidence for selective loss of cholinergic neurons in the nucleus basalis. *Annals of Neurology*, 10, 122–126. https://doi.org/10.1002/ana.410100203

Young, A. P., & Denovan-Wright, E. M. (2022). Synthetic cannabinoids reduce the inflammatory activity of microglia and subsequently improve neuronal survival in vitro. *Brain, Behavior, and Immunity*, 105, 29–43. https://doi.org/10.1016/j.bbi.2022.06.011

Zhou, F. W., & Puche, A. C. (2021). Short-term plasticity in cortical GABAergic synapses on olfactory bulb granule cells is modulated by endocannabinoids. *Frontiers in Cellular Neuroscience*, 15, 629052. https://doi.org/10.3389/fncel.2021.629052

SUPPORTING INFORMATION

Additional supporting information can be found online in the Supporting Information section at the end of this article.